Structural Engineering and Mechanics, *Vol. 58, No. 1 (2016) 59-91*
DOI: http://dx.doi.org/10.12989/sem.2016.58.1.059

Buckling of thick deep laminated composite shell of revolution under follower forces

Majid Khayat[1a], Davood Poorveis[*1], Shapour Moradi[2b] and Mona Hemmati[1c]

[1]*Department of Civil Engineering, Shahid Chamran University, Golestan Blvd., 61357831351, Ahvaz, Iran*
[2]*Department of Mechanical Engineering, Shahid Chamran University, Golestan Blvd., 61357831351, Ahvaz, Iran*

(Received September 11, 2015, Revised January 1, 2016, Accepted January 11, 2016)

Abstract. Laminated composite shells are commonly used in various engineering applications including aerospace and marine structures. In this paper, using semi-analytical finite strip method, the buckling behavior of laminated composite deep as well as thick shells of revolution under follower forces which remain normal to the shell is investigated. The stiffness caused by pressure is calculated for the follower forces subjected to external fibers in thick shells. The shell is divided into several closed strips with alignment of their nodal lines in the circumferential direction. The governing equations are derived based on first-order shear deformation theory which accounts for through thickness-shear flexibility. Displacements and rotations in the middle surface of shell are approximated by combining polynomial functions in the meridional direction as well as truncated Fourier series with an appropriate number of harmonic terms in the circumferential direction. The load stiffness matrix which accounts for variation of loads direction will be derived for each strip of the shell. Assembling of these matrices results in global load stiffness matrix which may be un-symmetric. Upon forming linear elastic stiffness matrix called constitutive stiffness matrix, geometric stiffness matrix and load stiffness matrix, the required elements for the second step analysis which is an eigenvalue problem are provided. In this study, different parameter effects are investigated including shell geometry, material properties, and different boundary conditions. Afterwards, the outcomes are compared with other researches. By considering the results of this article, it can be concluded that the deformation-dependent pressure assumption can entail to decrease the calculated buckling load in shells. This characteristic is studied for different examples.

Keywords: thick deep shell; laminated composite; follower force; finite strip method; buckling

1. Introduction

Once a structural model is subjected to a follower force, the strength direction will change due to structural deformation. Meanwhile, the model may experience divergence, flutter or both of

∗Corresponding author, Professor, E-mail: dpoorveis@scu.ac.ir
[a]M. Sc. Student, E-mail: khayatmajid@yahoo.com
[b]Professor, E-mail: moradis@scu.ac.ir
[c]M.Sc. Student, E-mail: Hemmati_m@yahoo.com

http://www.techno-press.org/?journal=sem&subpage=8 ISSN: 1225-4568 (Print), 1598-6217 (Online)

these instabilities which depend on structural conditions. Some of the most important applications of live pressure loading are: the aerodynamic drag forces acting on the body of rocket, the missiles and wings of aircraft carrying jet engines subject to follower forces, the forces acting on the rotor of a gas turbine, hydrostatic pressure and automobile disk brakes.

Fiber-reinforced composite materials are extensively used in laminated thick-walled weight-sensitive structural parts of various modern engineering structure in the aerospace, mechanical and civil engineering.

The buckling phenomenon consists of a sudden change of equilibrium configuration at a certain critical load. Buckling has crucial role in the behavior of thin structures such as plates and shells. Since the load carrying capacity of thin-walled members is frequently governed by the buckling phenomenon, the ability to calculate the associated elastic critical loads is of great importance. In addition, if a linear initial equilibrium path is assumed, linearized stability analysis reduces the determination of the critical load to a linear eigenvalue problem (Euler's method) (Nali *et al*. 2011).

Thangam *et al*. (1973) evaluated the natural frequency of a cylindrical panel which has simply supported ends by applying finite strip method. In their study, harmonic functions have been used in longitudinal direction. To predict the displacement functions in transverse direction, polynomial functions have been utilized. Classical plate theory plays a role in their research, as well. Chen and Zhang (1993) used finite strip method to evaluate buckling in the composite cylindrical shells reinforced by rings along with simply supported ends. By calculating the eigenvalues, buckling loads were obtained for different modes. In addition, the T-shaped and hat-shaped stiffness have been applied in the study. In another investigation, using semi-analytical finite strip method, Zhong and Cheung (1998) analyzed the prismatic structures. Therefore, they used the harmonic functions in longitudinal direction of strip. Next, buckling of composite shells was investigated by solving eigenvalue problem as the method was introduced by Wang and Dawe (1999) investigated the buckling of composite shell structures by the finite strip method. They used the first-order shear deformation and thin shell theory to buckling analysis. The case study in this article was laminated structures having arbitrary boundary conditions. Chen *et al*. (2000) presented a nonlinear geometric analysis by using semi-analytical finite strip method for composite plates subjected to vertical dynamic loads. The boundary conditions were simply support. The first-order shear deformation theory has been utilized. Moreover, to solve nonlinear equations, Newton-Raphson method has been used for isotropic and orthotropic plates. In another study, Dooms *et al*. (2004) simulated a thin-walled cylindrical structure by using two-dimensional (2-D) finite strip method. Consequently, they calculated the natural frequency at presence of lateral wind effect. Using finite strip method, Ovesy and Fazilati (2009) evaluated the stability of composite plates and cylindrical composite shells. In their study, post-buckling path was calculated by a nonlinear analysis. Afterwards, the critical buckling load was achieved through applying a linear analysis and Sanders (1959) relations. The boundary conditions at the both end and in along the length were simply supported. In addition, the first-order shear deformation theory has been applied in their study. Spagnoli (2001) calculated different buckling modes once conical thin-walled shells with longitudinal stiffeners are instable under axial pressure. To simulate structural model as well as reinforcements, 9-node Lagrangian shell element having five degrees of freedom has been utilized. In addition, the critical buckling load was calculated by using eigenvalue analysis. Ross and Little (2007) accomplished empirical tests to calculate plastic buckling load for cylindrical shells which were reinforced by ring stiffeners under uniform hydrostatic pressure. In addition, small deformation assumption played an effective role in elastic analysis. Tornabene *et*

al. (2014) evaluated the free vibration of free-form doubly-curved shells made of functionally graded materials using higher-order equivalent single layer theories. Tornabene *et al*. (2014) used the local the Generalized Differential Quadrature method applied to general higher-order theories of doubly-curved laminated composite shells to analysis the free vibration. Tornabene *et al*. (2015) used higher-order theories for the free vibrations of doubly-curved laminated panels with curvilinear reinforcing fibers by means of a local version of the the Generalized Differential Quadrature method. Tornabene *et al*. (2015) used the Generalized Differential quadrature method and shell theories of different order to studied free vibrations of laminated cylinders of oval and elliptic cross-sections.

On the other hand, thick shells have also extensive applications in different industries. Therefore, many researches have been conducted in this area. Wang and Schweizerhof (1996) established a boundary integral equation formulation of free vibration of moderately thick orthotropic laminated shallow shells by using the method of weighted residuals and the static fundamental solutions. In formulation of this study, the effects of neglecting the in-plane inertia and the rotatory inertia, singly and in combination are also considered. The boundary integral equations presented are reduced to a standard algebraic eigenvalue problem by means of boundary-domain elements. Heppler and Hansen (1986) derived a strain-displacement relation of the Reissner-Mindlin type for a general shell element which may be used equal confidence and ease in either plate or shell configurations over a wide range of thicknesses. The usual assumptions pertaining to thin and shallow shell geometry has not been employed resulting in strain-displacement relations which are consistent with the Reissner-Mindlin hypotheses for thick shell configurations. Kasagi and Sridharan (1993) analyzed thick composite-layered shells under hydrostatic pressure for buckling and post-buckling response using axisymmetric solid elements. The numerical approach was based on p-version finite elements in conjunction with appropriate trigonometric functions. Particular attention was given to the evaluation of inter laminar stresses in the post-buckling range. The post buckling response was determined using an asymptotic approach. Chao *et al*. (1988) used the semi-analytical solution for the axisymmetric buckling for perfect complete thick orthotropic spherical shells and hemispherical shells under various edge conditions subjected to uniform full external pressures. The solutions were achieved directly by using the Ritz method without considering the force as well as moment equilibrium and solving the complicated governing equations. Critical buckling loads and the various modes were found from the equations by using orthogonality and integral relations. Kang (2012) presented a three-dimensional (3-D) method of analysis to determine the free vibration frequencies of joined thick conical-cylindrical shells of revolution having variable thickness. Unlike conventional shell theories, which are mathematically 2-D, the study was based upon the 3-D dynamic equations of elasticity. Lu and Mao (2001) used a thick shell theory to calculate the critical load of plastic buckling of axially compressed cylindrical shells. The buckling equations were derived using the principle of virtual work on the basis of a transverse shear deformable displacement field. The deformation theory of plasticity was used for constitutive equations. Ross *et al*. (1999) described a theoretical and an experimental study into the collapse of three thick walled circular conical shells, which were tested to failure under external hydrostatic pressure. Two theoretical analyses were carried out which both were based on the finite element method. One of the theoretical analyses was based on inelastic non-symmetric bifurcation buckling and the other analysis was based on plastic axisymmetric buckling. Casimir *et al*. (2007) described a procedure for calculating the dynamic stiffness matrix of tubular shells with free edge boundary conditions. Such an analysis forms the basis for the continuous element method. The method was used to formulate a thick

axisymmetric shell element which takes into account rotatory inertia, transverse shear deformation and non-axisymmetric loadings. Kang and Leissa (2005) presented a three-dimensional 3-D method of analysis for determining the free vibration frequencies and mode shapes of thick, hyperboloidal shells of revolution. Unlike conventional shell theories, which are mathematically 2-D, the method was based upon the 3-D dynamic equations of elasticity. Kang (2015) used a three-dimensional method for determining the natural frequencies of a truncated shallow and deep conical shell with linearly varying thickness along the meridional direction free at its top edge and clamped at its bottom edge. Wang and Redekop (2011) analyzed the free vibration of moderately-thick of toroidal shell based on a shear deformation shell theory by differential quadrature method. Tornabene *et al*. (2015) studied the free vibration nature of laminated composite thick and moderately thick elliptic cones, cylinders and plates. They used Generalized differential quadrature (GDQ) method. Tornabene *et al*. (2015) estimated the behavior of doubly-curved composite deep shells with variable radii of curvature under concentrated loads by a new approach. The paper showed convergence, stability and accuracy of the present approach when applied to beams, plates and doubly-curved thin and thick shells. Tornabene *et al*. (2015) evaluated a comparison between classical 2-D and 3-D finite elements (FEs), classical and refined 2D generalized differential quadrature (GDQ) methods and an exact three-dimensional solution for analysis of free vibration of cylindrical and spherical shell panels.

Moreover, many researchers have investigated displacement dependent pressure. Bolotin (1963) was one of the pioneering researchers who studied the effects of load behavior on structures stability. He divided the loads into dead and follower types. The dead type remains constant both in magnitude and in direction. The follower load while remaining constant in magnitude but rotates in such a way that angle formed by the vector of the load and the normal to the shell surface follows a specific law. He also extracted the condition for uniformly distributed load over some part of the external surface of a body which remains normal to the deformed surface. In addition, he concluded that if the forces are non-conservative the form which the loss of stability assumes requiring special investigation in each problem. Both forms of instability are possible in this case. In a number of problems, depending on the relation between the parameters, the minimum critical loads can correspond to either the static or the oscillatory (flutter) forms of loss of stability. Another research which studied conservativeness of a normal pressure field acting on a shell, has been accomplished by Cohen (1966). He not only confirmed the Bolotin's research for flat plates but also generalized the results to a non-uniform continuous normal pressure field acting on an arbitrary shell. Afterwards, he modified the potential energy of loading to incorporate shells of arbitrary curvature. Romano (1971) extracted through the potential operator theory to present the correct proof of conservativeness condition. The analysis was performed in the large (finite deformation) obtaining a general condition for conservativeness of pressure loading. Sheinman and Tene (1974) emphasized on the functional potential energy derived by Cohen (1966); however, they suggested another expression for the normal pressure potential energy. Hibbitt (1979) extracted the contribution of follower forces to the tangent stiffness matrix which can be called load stiffness matrix. Generally, this matrix is un-symmetric but in special cases, it can appear as a symmetrical matrix. Due to non-uniform pressure, the investigator also demonstrated that the magnitude of non-symmetric matrix can be decreased by refining meshes while other aspects of non-symmetry are not dependent on element sizes. Schweizerhof and Ramm (1984) studied displacement-dependent pressure loads in nonlinear finite element analysis. They evaluated specific conditions when a pressure load is conservative and vice versa. The important part of their work was to propose a load classification into body attached and space attached loads. In the body

attached case, load stiffness matrix was divided into four parts so that three parts including two parts containing integrals along boundaries and the other related to variation of loading magnitude in the domain were skew-symmetric matrices. In the case of uniform pressure, the potential conditions were similar to those obtained by other researches. Altman *et al*. (1988-1990) studied vibration and stability of cylindrical shell panels under follower forces. The obtained solution (eigen curves) was used in conjunction with the dynamic criterion of stability to find the critical values of the frequency and loading parameters. Iwata *et al*. (1991) derived a symmetric load-stiffness matrix for buckling analysis of shell structures under uniform pressure loads. It should be noted that in finite element method, in order to execute large deformation analysis and to calculate the buckling load, it is necessary to introduce a load-stiffness or load correction matrix as well as the conventional linear and geometrically non-linear (initial stress) stiffness matrices. Therefore, they used the results obtained by Schweizerhof and Ramm (1984). Poorveis and Kabir (2006) estimated buckling of discretely stringer-stiffened composite cylindrical shells under combined axial compression and external pressure in the form of live (follower) pressure. Cagdas and Adali (2011) investigated buckling of cross-ply cylinders under hydrostatic pressure by considering pressure stiffness and regarding semi-analytical finite element method. They studied the effects of pressure stiffness for different lay-ups and geometries. Park and Kim (2002) tried to reasonably simulate behavior of rockets or missile. They analyzed dynamic stability of completely free cylindrical shells under axial follower force for a specific situation in which the edge of shell is movable but not freely deformable. By executing geometric nonlinear analysis, Lazzari *et al*. (2003) carried out the study of large lightweight roof structures under the dynamic effects of the turbulent actions caused by wind. The wind loads were considered as deformation-dependent forces. Wang (2003) studied a beam structure subjected to a static follower force. The beam was fixed in the transverse direction and constrained by a rotational spring at one end, and by a translational spring and a rotational spring at the other end. Fukuchi and Tanaka (2006) investigated non-periodic motions and fractals of a circular arch under follower forces with small disturbances. The stability region chart of the disturbed equilibrium in an excitation field was calculated numerically.

In this study, we propose a method to determine the effects of follower forces on buckling analysis of composite shells of revolution. In this regard, in order to calculate the pressure stiffness, the article proposes a procedure which is novel compared to prior methods. Prior studies have investigated the follower forces subjected to neutral axis. This assumption may not be appropriate in the general case, dealing with thick shells. Two factors can affect on the response of thick shell in this regard. First, applying loading on external surface or middle surface of the shell resulting different pre-buckling stresses and second, the deformation that will be experienced in each case through the buckling process can be dissimilar. Therefore, this article considers the subjected follower force on external fiber and suggests a general pressure stiffness matrix for every thick shells of revolution.

2. Methodology

2.1 Shell geometry and coordinate system

The position of each shell point is introduced by a circumferential component (θ), a meridional component (φ), and a normal coordinate (z) to the middle surface illustrated in Fig. 1.

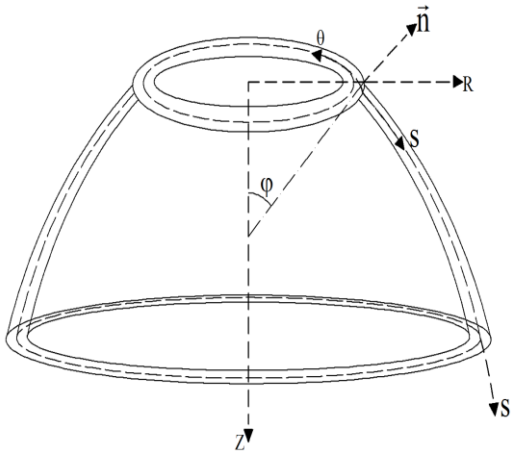

Fig. 1 Coordinate system

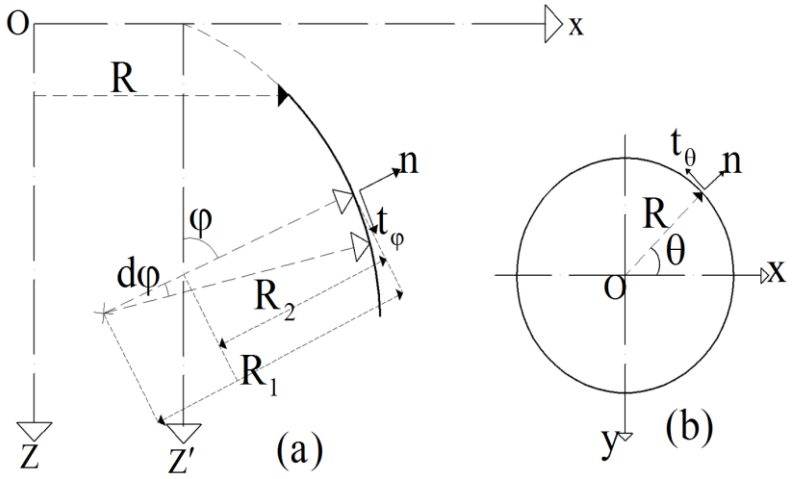

Fig. 2 Geometry of shell of revolution: (a) meridional section; (b)circumferential section

The angle formed by the extended normal to the surface and the *z*- axis rotation of the meridian curve is defined as the meridional angle (φ) and the angle between the radius of the parallel circle and the *x*-axis is designated as the circumferential angle (θ) as shown in Fig. 2. The parametric co-ordinates are defined as (θ, φ), respectively. Each point distance from the mid-surface of the shell along the normal axis is *z*. The total thickness of the shell is also represented by *h* (Tornabene and Viola 2008).

It should be noted that, owing to weakness of composite material in shear deformation, in this article, the first-order shear deformation theory has been utilized. Therefore, the displacement field corresponding to the first order shear deformation theory is given as

$$\begin{aligned} \bar{u}(s,\theta,z) &= u(s,\theta) + z\beta_s(s,\theta) \\ \bar{v}(s,\theta,z) &= v(s,\theta) + z\beta_\theta(s,\theta) \\ \bar{w}(s,\theta,z) &= w(s,\theta) \end{aligned} \tag{1}$$

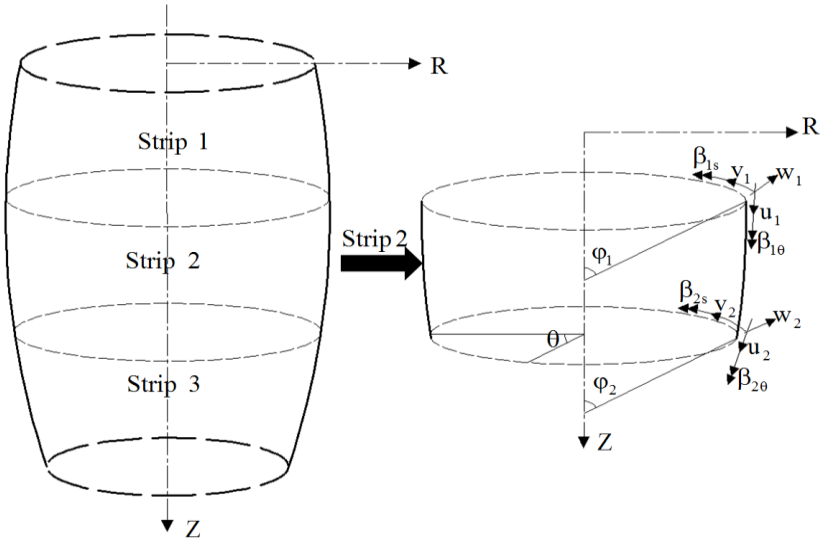

Fig. 3 Strip method-discretization

where: u, v and w are displacements in the middle plane of the laminate and β_s, β_θ are the rotations of the normal axis the middle plane around the θ and s axes, respectively.

2.2 Semi analytical method (Finite strip method)

The shell is divided into several closed strips being aligned with their nodal lines in the circumferential direction (Fig. 3). Displacements and rotations in the middle surface of shell are approximated by combining polynomial functions in the meridional direction and truncated Fourier series having appropriate number of harmonic term in the circumferential direction.

The circumferential variables of the global displacements u, v, w, β_s and β_θ can be described by a suitable Fourier series expansion which generally consists of both symmetric and anti-symmetric terms

$$
\begin{aligned}
u(s,\theta,t) &= u^{c_o}(s) + \sum_{k=1}^{NH}\left[u^{c_n}(s)\cos(kn_{cr}\theta) + u^{s_n}(s)\sin(kn_{cr}\theta)\right] \\
v(s,\theta,t) &= v^{c_o}(s) + \sum_{k=1}^{NH}\left[v^{c_n}(s)\cos(kn_{cr}\theta) + v^{s_n}(s)\sin(kn_{cr}\theta)\right] \\
w(s,\theta,t) &= w^{c_o}(s) + \sum_{k=1}^{NH}\left[w^{c_n}(s)\cos(kn_{cr}\theta) + w^{s_n}(s)\sin(kn_{cr}\theta)\right] \\
\beta_s(s,\theta,t) &= \beta_s^{c_o}(s) + \sum_{k=1}^{NH}\left[\beta_s^{c_n}(s)\cos(kn_{cr}\theta) + \beta_s^{s_n}(s)\sin(kn_{cr}\theta)\right] \\
\beta_\theta(s,\theta,t) &= \beta_\theta^{c_o}(s) + \sum_{k=1}^{NH}\left[\beta_\theta^{c_n}(s)\cos(kn_{cr}\theta) + \beta_\theta^{s_n}(s)\sin(kn_{cr}\theta)\right]
\end{aligned}
\tag{2}
$$

where θ stands for the circumferential angular coordinate, k represents a coefficient and NH is the number of terms in the truncated series, c_n and s_n are coefficients of Fourier series and n_{cr} is the

circumferential wave number. The displacement and rotation expansions apply for both pre-buckling state and buckling modes. The number of harmonics used in the analyses depends on the subjected loads as well as material anisotropy. In the case of uniform axisymmetric, axial or lateral pressure and material isotropy, only axisymmetric terms are active in the pre-buckling state. On the other hand, for buckling mode, only one wave number which leads to the minimum buckling loads is involved in the analysis. Generally, when a shell made by coupling material stiffness is subjected to partial deformation dependent loadings, full expansions are required for both pre-buckling and buckling states.

2.3 Thick shell theory

The equations include accurate force and moment resultant relations for laminated composite deep thick shells where the $1+z/R$ (R is radius of shell) terms are considered in the stress resultant equations and integrated precisely (Asadi *et al*. 2012). The strain-displacement relationships at any arbitrary point of the shell thickness can be expressed as follows

$$\begin{aligned}
&\bar{\varepsilon}_{ss} = \frac{1}{(1+z/R_1)}(\varepsilon_{ss} + zk_{ss}) \qquad \bar{\varepsilon}_{\theta\theta} = \frac{1}{(1+z/R_2)}(\varepsilon_{\theta\theta} + zk_{\theta\theta}) \quad \bar{\varepsilon}_{zz} = 0 \\
&\bar{\varepsilon}_{s\theta} = \frac{1}{(1+z/R_1)}(\varepsilon_{s\theta} + zk_{s\theta}) \qquad \bar{\varepsilon}_{\theta s} = \frac{1}{(1+z/R_2)}(\varepsilon_{\theta s} + zk_{\theta s}) \\
&\bar{\varepsilon}_{sz} = \frac{1}{(1+z/R_1)}(\gamma_{sz} - z(\beta_{\theta z}/R_{12})) \qquad \bar{\varepsilon}_{\theta z} = \frac{1}{(1+z/R_2)}(\gamma_{\theta z} - z(\beta_{sz}/R_{12}))
\end{aligned} \tag{3}$$

where, linear strains of mid-plane and curvatures, based on Qatu (1999), Asadi *et al*. (2012) and Teng (1998) investigations, are as follows

$$\varepsilon_{ss}^{l} = \frac{1}{A_1}\frac{\partial u}{\partial \varphi} + \frac{1}{A_1A_2}\frac{\partial A_1}{\partial \theta}v + \frac{w}{R_1}$$

$$\varepsilon_{\theta\theta}^{l} = \frac{1}{A_2}\frac{\partial v}{\partial \theta} + \frac{1}{A_1A_2}\frac{\partial A_2}{\partial \varphi}u + \frac{w}{R_2}$$

$$\varepsilon_{s\theta}^{l} = \frac{1}{A_1}\frac{\partial v}{\partial \varphi} + \frac{1}{A_2}\frac{\partial u}{\partial \theta} - \frac{1}{A_1A_2}\frac{\partial A_2}{\partial \varphi}v - \frac{1}{A_1A_2}\frac{\partial A_1}{\partial \theta}u$$

$$\varepsilon_{\theta s}^{l} = \frac{1}{A_1}\frac{\partial v}{\partial \varphi} + \frac{1}{A_2}\frac{\partial u}{\partial \theta} - \frac{1}{A_1A_2}\frac{\partial A_2}{\partial \varphi}v - \frac{1}{A_1A_2}\frac{\partial A_1}{\partial \theta}u$$

$$\varepsilon_{sz} = \beta_{sz} + \frac{1}{A_1}\frac{\partial w}{\partial \varphi} - \frac{u}{R_1}$$

$$\varepsilon_{\theta z} = \beta_{\theta z} + \frac{1}{A_2}\frac{\partial w}{\partial \theta} - \frac{v}{R_2}$$

$$k_{ss} = \frac{1}{A_1}\frac{\partial \beta_s}{\partial \varphi} + \frac{1}{A_1A_2}\frac{\partial A_1}{\partial \theta}\beta_\theta$$

$$k_{\theta\theta} = \frac{1}{A_2}\frac{\partial \beta_\theta}{\partial \theta} + \frac{1}{A_1A_2}\frac{\partial A_2}{\partial \varphi}\beta_s$$

$$k_{s\theta} = \frac{1}{A_1}\frac{\partial \beta_\theta}{\partial \varphi} - \frac{1}{A_1A_2}\frac{\partial A_2}{\partial \varphi}\beta_s + \frac{1}{A_2}\frac{\partial \beta_s}{\partial \theta} + \frac{1}{2A_1A_2}\left(\frac{\partial (A_2 v)}{\partial \varphi} - \frac{\partial (A_1 u)}{\partial \theta}\right)\left(\frac{1}{R_1} - \frac{1}{R_2}\right)$$

$$k_{\theta s}=\frac{1}{A_1}\frac{\partial\beta_\theta}{\partial\varphi}-\frac{1}{A_1A_2}\frac{\partial A_2}{\partial\varphi}\beta_s+\frac{1}{A_2}\frac{\partial\beta_s}{\partial\theta}+\frac{1}{2A_1A_2}\left(\frac{\partial(A_2v)}{\partial\varphi}-\frac{\partial(A_1u)}{\partial\theta}\right)\left(\frac{1}{R_1}-\frac{1}{R_2}\right) \tag{4}$$

R_{12} is the radius of twist curvature and A_1 and A_2 are lame's parameters and calculated according to R_1 and R_2 (Fig. 2)

$$A_1=R_1 \quad A_2=R_2\sin\varphi=R \tag{5}$$

Non-linear strains are

$$\begin{aligned}
\varepsilon_{ss}^{nl}&=\frac{1}{2}\left(\frac{1}{A_1}\frac{\partial w}{\partial\varphi}-\frac{u}{R_1}\right)^2+\frac{1}{2}\left(\frac{1}{2A_1A_2}\left(\frac{\partial(A_2v)}{\partial\varphi}-\frac{\partial(A_1u)}{\partial\theta}\right)\right)^2\\
\varepsilon_{\theta\theta}^{nl}&=\frac{1}{2A_2^{\,2}}\left(\frac{\partial w}{\partial\theta}-v\sin\varphi\right)^2+\frac{1}{2}\left(\frac{1}{2A_1A_2}\left(\frac{\partial(A_2v)}{\partial\varphi}-\frac{\partial(A_1u)}{\partial\theta}\right)\right)^2\\
\varepsilon_{s\theta}^{nl}&=\left(\frac{1}{A_1}\frac{\partial w}{\partial\varphi}\right)\left(\frac{1}{A_2}\frac{\partial w}{\partial\theta}-\frac{v}{R_2}\right)\\
\varepsilon_{\theta s}^{nl}&=\left(\frac{u}{R_1}\right)\left(\frac{1}{A_2}\frac{\partial w}{\partial\theta}-\frac{v}{R_2}\right)
\end{aligned} \tag{6}$$

The stress-strain relation for a single orthotropic lamina in a shell is

$$\begin{Bmatrix}\sigma_{ss}\\ \sigma_{\theta\theta}\\ \sigma_{zz}\\ \sigma_{\theta z}\\ \sigma_{sz}\\ \sigma_{s\theta}\end{Bmatrix}=\begin{bmatrix}\bar{Q}_{11}&\bar{Q}_{12}&\bar{Q}_{13}&0&0&\bar{Q}_{16}\\ \bar{Q}_{12}&\bar{Q}_{22}&\bar{Q}_{23}&0&0&\bar{Q}_{26}\\ \bar{Q}_{13}&\bar{Q}_{23}&\bar{Q}_{33}&0&0&\bar{Q}_{36}\\ 0&0&0&\bar{Q}_{44}&\bar{Q}_{45}&0\\ 0&0&0&\bar{Q}_{45}&\bar{Q}_{55}&0\\ \bar{Q}_{16}&\bar{Q}_{26}&\bar{Q}_{36}&0&0&\bar{Q}_{66}\end{bmatrix}\begin{Bmatrix}\varepsilon_{ss}\\ \varepsilon_{\theta\theta}\\ \varepsilon_{zz}\\ \varepsilon_{\theta z}\\ \varepsilon_{sz}\\ \varepsilon_{s\theta}\end{Bmatrix} \tag{7}$$

where $\bar{Q}_{ij}$ is the reduced transformed stiffness (Qatu 1999, Asadi *et al*. 2012). The force and moment resultants are obtained by integrating the stresses over the shell thickness. The normal and shear force resultants are presented in Qatu (1999), Asadi *et al*. (2012) (Fig. 4)

$$\begin{Bmatrix}N_{ss}\\ N_{s\theta}\\ Q_{sz}\end{Bmatrix}=\int_{-h/2}^{h/2}\begin{Bmatrix}\sigma_{ss}\\ \sigma_{s\theta}\\ \sigma_{sz}\end{Bmatrix}(1+z/R_1)dz$$

$$\begin{Bmatrix}N_{\theta\theta}\\ N_{\theta s}\\ Q_{\theta z}\end{Bmatrix}=\int_{-h/2}^{h/2}\begin{Bmatrix}\sigma_{\theta\theta}\\ \sigma_{s\theta}\\ \sigma_{\theta z}\end{Bmatrix}(1+z/R_2)dz \tag{8}$$

The bending and twisting moment resultants as well as higher-order shear resultant terms are expressed as

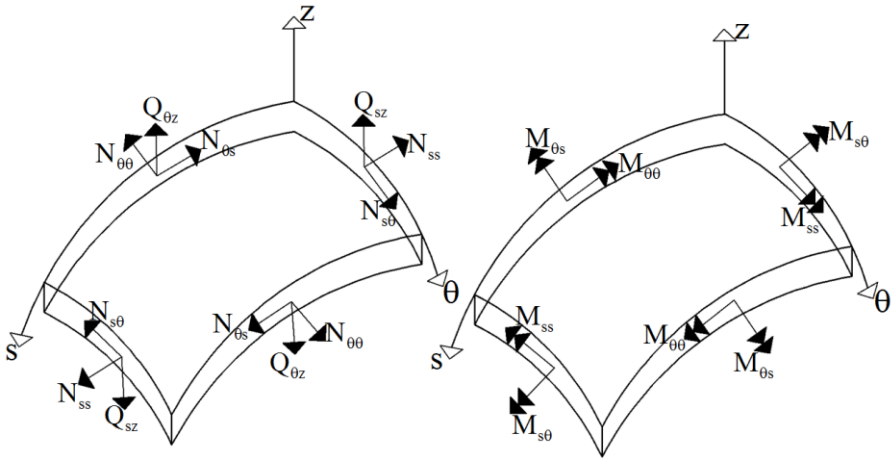

Fig. 4 Force resultants and moments

$$\begin{Bmatrix} M_{ss} \\ M_{s\theta} \\ P_{s\theta} \end{Bmatrix} = \int_{-h/2}^{h/2} \begin{Bmatrix} \sigma_{ss} \\ \sigma_{s\theta} \\ \sigma_{sz} \end{Bmatrix} (1+z/R_1) z dz$$
$$\begin{Bmatrix} M_{\theta\theta} \\ M_{\theta s} \\ P_{\theta s} \end{Bmatrix} = \int_{-h/2}^{h/2} \begin{Bmatrix} \sigma_{\theta\theta} \\ \sigma_{s\theta} \\ \sigma_{sz} \end{Bmatrix} (1+z/R_2) z dz \tag{9}$$

where $P_{s\theta}$ and $P_{\theta s}$ are higher-order shear terms; they need the state only if the radius of twist curvature exists. In this paper similar to (Qatu 1999, Asadi *et al*. 2012), exact stress resultants are obtained when the term is included and the integration is precisely carried out. The constitutive equations relate internal stress resultants and internal couples with generalized strain components on the middle surface

$$\begin{Bmatrix} N_{ss} \\ N_{\theta\theta} \\ N_{s\theta} \\ N_{\theta s} \\ M_{ss} \\ M_{\theta\theta} \\ M_{s\theta} \\ M_{\theta s} \end{Bmatrix} = \begin{bmatrix} \overline{A}_{11} & A_{12} & \overline{A}_{16} & A_{16} & \overline{B}_{11} & B_{12} & \overline{B}_{16} & B_{16} \\ A_{12} & \hat{A}_{22} & A_{26} & \hat{A}_{26} & B_{11} & \hat{B}_{22} & B_{26} & \hat{B}_{26} \\ \overline{A}_{16} & A_{26} & \overline{A}_{66} & A_{66} & \overline{B}_{16} & B_{26} & \overline{B}_{66} & B_{66} \\ A_{16} & \hat{A}_{26} & A_{66} & \hat{A}_{66} & B_{16} & \hat{B}_{26} & B_{66} & \hat{B}_{66} \\ \overline{B}_{11} & B_{12} & \overline{B}_{16} & B_{16} & \overline{D}_{11} & D_{12} & \overline{D}_{16} & D_{16} \\ B_{11} & \hat{B}_{22} & B_{26} & \hat{B}_{26} & D_{11} & \hat{D}_{22} & D_{26} & \hat{D}_{26} \\ \overline{B}_{16} & B_{26} & \overline{B}_{66} & B_{66} & \overline{D}_{16} & D_{26} & \overline{D}_{66} & D_{66} \\ B_{16} & \hat{B}_{26} & B_{66} & \hat{B}_{66} & D_{16} & \hat{D}_{26} & D_{66} & \hat{D}_{66} \end{bmatrix} \begin{Bmatrix} \varepsilon_{ss} \\ \varepsilon_{\theta\theta} \\ \varepsilon_{s\theta} \\ \varepsilon_{\theta s} \\ k_{ss} \\ k_{\theta\theta} \\ k_{s\theta} \\ k_{\theta s} \end{Bmatrix}$$
$$\begin{Bmatrix} Q_{ss} \\ Q_{\theta\theta} \\ P_{s\theta} \\ P_{\theta s} \end{Bmatrix} = \begin{bmatrix} \overline{A}_{44} & A_{45} & \overline{B}_{44} & B_{45} \\ A_{45} & \hat{A}_{55} & B_{45} & \hat{B}_{55} \\ \overline{B}_{44} & B_{45} & \overline{D}_{44} & D_{45} \\ B_{45} & \hat{B}_{55} & D_{45} & \hat{D}_{55} \end{bmatrix} \begin{Bmatrix} \varepsilon_{sz} \\ \varepsilon_{\theta z} \\ -\beta_{ss}/R_{12} \\ -\beta_{\theta\theta}/R_{12} \end{Bmatrix} \tag{10}$$

A_{ij} is extensional stiffness, D_{ij} is bending stiffness and B_{ij} is bending-extensional coupling stiffness are defined as

$$\left.\begin{aligned}
\bar{A}_{ij} &= A_{ij} - \left(\frac{1}{R_1} - \frac{1}{R_2}\right)B_{ij} \qquad \hat{A}_{ij} = A_{ij} + \left(\frac{1}{R_1} - \frac{1}{R_2}\right)B_{ij} \\
\bar{B}_{ij} &= B_{ij} - \left(\frac{1}{R_1} - \frac{1}{R_2}\right)D_{ij} \qquad \hat{B}_{ij} = B_{ij} + \left(\frac{1}{R_1} - \frac{1}{R_2}\right)D_{ij} \\
\bar{D}_{ij} &= D_{ij} - \left(\frac{1}{R_1} - \frac{1}{R_2}\right)E_{ij} \qquad \hat{D}_{ij} = D_{ij} + \left(\frac{1}{R_1} - \frac{1}{R_2}\right)E_{ij}
\end{aligned}\right\} \; i, j = 1, 2, 4, 6, 5$$

$$\left.\begin{aligned}
A_{ij} &= \sum_{k=1}^{N} \bar{Q}_{ij}^{(k)}(h_k - h_{k-1}) \\
B_{ij} &= \frac{1}{2}\sum_{k=1}^{N} \bar{Q}_{ij}^{(k)}(h_k^2 - h_{k-1}^2) \\
D_{ij} &= \frac{1}{3}\sum_{k=1}^{N} \bar{Q}_{ij}^{(k)}(h_k^3 - h_{k-1}^3) \\
E_{ij} &= \frac{1}{4}\sum_{k=1}^{N} \bar{Q}_{ij}^{(k)}(h_k^4 - h_{k-1}^4)
\end{aligned}\right\} \; i, j = 1, 2, 6$$

$$\left.\begin{aligned}
A_{ij} &= \sum_{k=1}^{N} K_i K_j \bar{Q}_{ij}^{(k)}(h_k - h_{k-1}) \\
B_{ij} &= \frac{1}{2}\sum_{k=1}^{N} K_i K_j \bar{Q}_{ij}^{(k)}(h_k^2 - h_{k-1}^2) \\
D_{ij} &= \frac{1}{3}\sum_{k=1}^{N} K_i K_j \bar{Q}_{ij}^{(k)}(h_k^3 - h_{k-1}^3)
\end{aligned}\right\} \; i, j = 4, 5 \tag{11}$$

where K_i and K_j in the above equations are shear correction coefficients, typical taken at 5/6 (Qatu 1999).

2.4 Linear elastic and geometric stiffness matrices

To investigate the linear elastic stiffness matrix, the internal virtual work is calculated by using Eq. (12)

$$\delta W_{\text{int}}^{1} = \int_{\varphi}\int_{\theta}\int_{t} \left(\sigma_{ss}\delta\varepsilon_{ss}^{\,1} + \sigma_{\theta\theta}\delta\varepsilon_{\theta\theta}^{\,1} + \tau_{s\theta}\delta\gamma_{s\theta}^{\,1} + \tau_{\theta s}\delta\gamma_{\theta s}^{\,1} + \tau_{sz}\delta\gamma_{sz}^{\,1} + \tau_{\theta z}\delta\gamma_{\theta z}^{\,1}\right)\left(1+\frac{z}{R_1}\right)\left(1+\frac{z}{R_2}\right)A_1A_2\,dz\,d\theta\,d\varphi \tag{12}$$

By integration Eq. (12) on thickness, the virtual work is

$$\begin{aligned}
\delta W_{\text{int}}^{1} = \int_{s}\int_{\theta} & (N_{ss}\delta\varepsilon_{ss}^{\,1} + N_{\theta\theta}\delta\varepsilon_{\theta\theta}^{\,1} + N_{s\theta}\delta\varepsilon_{s\theta}^{\,1} + N_{\theta s}\delta\varepsilon_{\theta s}^{\,1} + M_{ss}\delta k_{ss}^{\,1} \\
& + M_{\theta\theta}\delta k_{\theta\theta}^{\,1} + M_{s\theta}\delta k_{s\theta}^{\,1} + M_{\theta s}\delta k_{\theta s}^{\,1} + Q_{ss}\delta\varepsilon_{sz}^{\,1} + Q_{\theta\theta}\delta\varepsilon_{\theta z}^{\,1})R\,d\theta\,ds
\end{aligned} \tag{13}$$

Also, the equation can be rewritten as below based on Eq. (13)

$$\delta W_{\text{int}}^{l} = (\delta\{\hat{\Delta}\})^{T}[K_e]\{\hat{\Delta}\} \tag{14}$$

where, K_e is linear elastic stiffness matrix, $\hat{\Delta}$ is displacements and rotations vector of shell and $\delta\hat{\Delta}$ is virtual displacements and rotations. In order to calculate the geometric stiffness matrix or initial stress, firstly, a static analysis is done for the pre-buckling state. Then, in-plane stresses including N^{o}_{ss}, $N^{o}_{s\theta}$, $N^{o}_{\theta s}$ and $N^{o}_{\theta\theta}$ are calculated. Finally, virtual work created by membrane forces, is introduced to investigate nonlinear virtual work as following

$$\delta W^{nl}_{int} = \int_{s}\int_{\theta} (N^{o}_{ss}\delta\varepsilon_{ss}{}^{nl} + N^{o}_{\theta\theta}\delta\varepsilon_{\theta\theta}{}^{nl} + N^{o}_{s\theta}\delta\varepsilon_{s\theta}{}^{nl} + N^{o}_{\theta s}\delta\varepsilon_{\theta s}{}^{nl})Rd\theta ds \tag{15}$$

Substituting nonlinear strains calculated by using the Eq. (6) to Eq. (15), geometric stiffness matrix K_G can be extracted by Eq. (16)

$$\delta W^{nl}_{int} = (\delta\{\hat{\Delta}\})^{T}[K_G]\{\hat{\Delta}\} \tag{16}$$

It should be mentioned that linear elastic stiffness matrix as well as geometric stiffness matrix have some harmonic dependent terms which have been utilized in displacement and rotation expansions. Also, because of using close shell assumption, integration is considered in the circumferential direction and based on different harmonic assumption.

2.5 Stiffness of pressure (uniform follower force)

As it was discussed before, in this article, the first-order shear deformation assumption plays a significant role in order to calculate the pressure stiffness. In the previous investigations, loads were subjected to the neutral axis in both thick and thin shells. Schweizerhof and Ramm (1984) categorized the follower forces in two groups: Body attached and Space attached. In the case of space attached, both their magnitude and direction change relative to the structural deformation. Whereas, only direction of body attached forces alter when the structural deformations occur. In

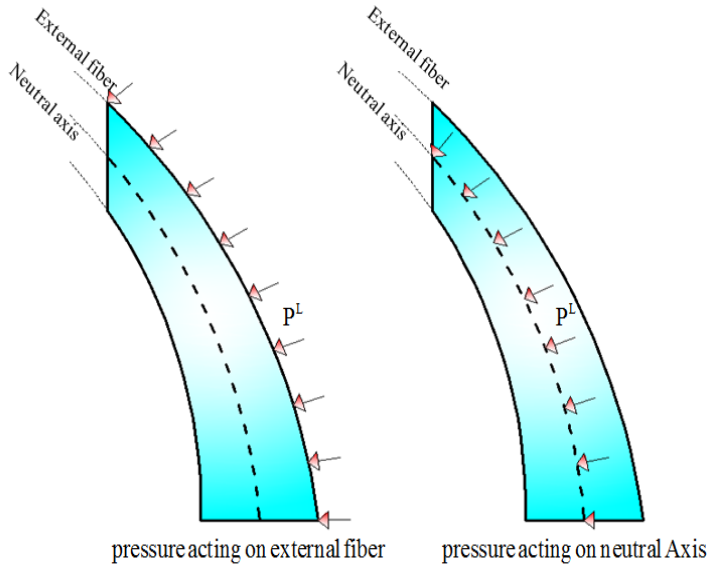

Fig. 5 Follower pressure acting on shell

this study, body attached assumption has been considered. It should also be mentioned that all the strain are in infinitesimal strain zone. Therefore, all the relations regarding the stiffness of pressure can be written for neutral axis as well as external fiber of the shell as presented in Fig. 5.

Fig. 6 reveals that if $\vec{R}$ is defined as the vector of an arbitrary shell point, which the point can located on neutral axis (z=0) or on external fiber of the shell (z=h/2), and $\vec{U}$ is the displacement vector of the supposed point, then after the deformations, the displacement vector ($\vec{R}^*$) can be calculated by using the Eq. (17).

$$\vec{R}^* = \vec{R} + \vec{U} \tag{17}$$

This equation can be redefined by considering the first-order shear theory and shell degrees of freedom as below (Fig. 2)

$$\begin{aligned}\overrightarrow{R^*} &= \left(R\cos\theta + u\cos\varphi\cos\theta - z\beta_s\cos\varphi\cos\theta + w\sin\varphi\cos\theta - v\sin\theta + z\beta_\theta\sin\theta\right)\vec{i} \\ &+ \left(R\sin\theta + u\cos\varphi\sin\theta - z\beta_s\cos\varphi\sin\theta + w\sin\varphi\sin\theta + v\cos\theta - z\beta_\theta\cos\theta\right)\vec{j} \\ &+ \left(Z + u\sin\varphi - z\beta_s\sin\varphi - w\cos\varphi\right)\vec{k}\end{aligned} \tag{18}$$

Virtual work caused by follower pressure can be calculated by the Eq. (19).

$$\delta W_{ext}^{ql} = \int_s\int_\theta \left(P^l dS^* \vec{n}^*\right)\cdot\delta\vec{U} \tag{19}$$

where dS^* is deformed elemental area, $\vec{n}^*$ is normal vector to the deformed area, P^l is follower force and $\delta\vec{U}$ is virtual displacement vector which can be estimated by Eq. (20):

$$\begin{aligned}\delta\vec{U} &= \left(\delta u - z\delta\beta_s\right)\vec{t} + (\delta w)\vec{n} + \left(\delta v - z\delta\beta_\theta\right)\vec{n}_\theta = \left(\delta u - z\delta\beta_s\right) \\ &\left(\cos\varphi\cos\theta\vec{i} + \cos\varphi\sin\theta\vec{j} + \sin\varphi\vec{k}\right) + \delta w\left(\sin\varphi\cos\theta\vec{i} + \sin\varphi\sin\theta\vec{j} - \cos\varphi\vec{k}\right) \\ &\left(\delta v - z\delta\beta_\theta\right)\left(-\sin\theta\vec{i} + \cos\theta\vec{j}\right)\end{aligned} \tag{20}$$

where $\overrightarrow{n_\theta}$ and $\vec{n}, \vec{t}$ are the unit vectors of circumferential, normal and meridional directions, respectively. Utilizing the vector analysis for calculating the elemental area and the normal vector of deformed structure, the following relation can be written

$$dS^*\vec{n}^* = \frac{\partial\vec{R}^*}{\partial\theta}d\theta \times \frac{\partial\vec{R}^*}{\partial s}ds \tag{21}$$

The reader can refer to appendix A to acquire more information regarding calculation of the elemental area and the normal vector of deformed structure. By using the Eq. (19) and the determinant expansion stated in the first appendix, external virtual expansion caused by the dependent- displacement lateral pressure the Eq. (21) is written where F_u, F_v, F_w, $F_{\beta\theta}$ and $F_{\beta s}$ are work counterpart of virtual displacements, u, v, w, β_θ and β_s, respectively (presented in appendix B).

$$\delta W_{ext}^{ql} = \int_0^{2\pi}\int_0^L P^l\left(F_u\delta u + F_v\delta v + F_w\delta w + F_{\beta_s}\delta\beta_s + F_{\beta_\theta}\delta\beta_\theta\right)Rdsd\theta \tag{22}$$

It should be mentioned that the reader can utilize the potential operator to separate the

symmetric parts of stiffness matrix which are caused by pressure from the non-symmetric parts. Firstly, the second-order and upper-order terms are eliminated since they have no effective role in constant pressure stiffness matrix. Next, performing integration by parts on some terms of Eq. (22) and using first variation operator to separate the potential function in the shell domain from the virtual work of boundaries (Eq. (23)).

$$\begin{aligned}\delta W_{foll}^{ql} = -\delta\int\int P^{l}(&\frac{u^2}{2R_1}+\frac{v^2}{2R}\sin\varphi+\frac{w^2}{2R}\sin\varphi+\frac{w^2}{2R_1}+\frac{w}{R}\frac{\partial v}{\partial\theta}+\frac{w}{R}\frac{\partial}{\partial s}(Ru)\\ &-\frac{z}{R_1}u\beta_s+\frac{z^2}{2R_1}\beta_s{}^2-\frac{w}{R}z\frac{\partial}{\partial s}(R\beta_s)+\frac{z^2}{2R}\beta_\theta{}^2\sin\varphi-z\frac{v}{R}\beta_\theta\sin\varphi-\frac{z}{R}w\frac{\partial\beta_\theta}{\partial\theta})Rdsd\theta\\ &-\int_0^{2\pi}P^{l}\left(\delta\beta_s wzR\right)_0^{l}d\theta+\int_0^{2\pi}P^{l}\left(w\delta uR\right)_0^{l}d\theta\end{aligned} \tag{23}$$

The external virtual work of uniform follower pressure on shell of revolution consists of two different parts (Eq. (23)): the first part includes several specific form potential functions. This part of external virtual work leads to symmetric pressure stiffness matrix. On the other hand, the second part is concerned about boundary conditions of shell ends. In other words, if shell is not sufficiently restrained in one of its end, pressure stiffness becomes non-symmetric. When the pressure stiffness matrix is symmetric, it is called conservative system but if the pressure stiffness matrix is un-symmetric, it is known as non-conservative system. In the case of conservative system, static criteria (divergence) can be used which finally produces symmetric global stiffness matrix. Non-conservativeness of loads can cause the system to be divided into purely and hybrid non-conservative. The first group only fails by flutter; consequently, the kinetic criteria, which connect computing buckling loads to vibration equation of structure, govern. In the hybrid case, both criteria, static or kinetic can dominate the problem (Argyris and Symeonidis 1981). In commercial programs such as Abaqus, pressure stiffness matrix is stored symmetrically (Goyal and Kapania 2008, ABAQUS/standard user's manual 1998). In all cases of this article, the static analysis (or divergence criterion) has been utilized in order to calculate the buckling load.

2.6 Eigenvalue problem

The pre-buckling stresses are determined by performing a primary static analysis for the structure under the given loading. The buckling load parameter λ_{cr} is defined as the ratio of the actual buckling load to the applied forces in the points where buckling occurs, is obtained by solving the eigenvalue problem as below. The buckling load parameter for the externally pressurized case can be obtained by solving the modified eigenvalue problem (Cagdas and Adali 2011)

$$\det\left[K_e-\lambda_{cr}\left(K_G\right)\right]=0 \tag{24}$$

The buckling parameter for follower pressure obtained by solving the modified eigenvalue problem

$$\det\left[K_e-\lambda_{cr}\left(K_G+K_p\right)\right]=0 \tag{25}$$

where K_e is the global linear stiffness matrix, K_G is the global geometric stiffness matrix, K_P is the global pressure stiffness and λ_{cr} is the lowest eigenvalue of the buckling load parameter. The

corresponding buckling pressure is equal

$$P_{cr} = \lambda_{cr} * P \tag{26}$$

3. Numerical results and discussion

3.1 Comparison results

In this example, the result of analysis is carried out for cylindrical shells with two fixed ends under a uniform pressure. Therefore, different properties such as shell thickness effects on buckling load, effects of length to radius ratio by considering the presence and absence of pressure stiffness (PS) on buckling load, and lay-ups ($[90/90/90]_s$, $[0/90/0]_s$) have been compared with other research results. The radius of the cylinder is 190.5 mm. The material properties also considered as follows:

$$E_{11} = 206.844 \text{ GPa} \quad E_{22} = 18.6159 \text{ GPa} \quad G_{12} = G_{13} = 4.482 \text{ GPa}$$
$$G_{23} = 2.55107 \text{ GPa} \quad \upsilon_{12} = \upsilon_{13} = 0.21 \quad \upsilon_{23} = 0.25$$

In this study, the difference of buckling loads, with the presence and absence of pressure stiffness, is calculated by Eq. (27)

$$\mu(\%) = \left| \frac{q_{cr(\text{without PS})} - q_{cr(\text{with PS})}}{q_{cr(\text{with PS})}} \right| * 100 \tag{27}$$

Table 1 Critical values of pressure (MPa) for clamped cylindrical shell and for various length to radius ratio (*L/R*) and thickness (*h*)

h	*L/R*	*n*	Cagdas and Adali (2011) without PS	Cagdas and Adali (2011) with PS	Cagdas and Adali (2011) μ(%)	Current study without PS	Current study with PS	μ(%)
				[90/90/90]s				
6.35	1	5	18.5	18	3.1	18.4	17.5	5.4
6.35	2	3	11.1	10	10.5	11	9.89	10.9
6.35	5	3	5.99	5.39	11.2	5.98	5.35	11.7
12.7	1	4	92.3	88.7	4.1	91.3	86.5	5.6
12.7	2	3	52.6	48.2	9	52	46.9	10.8
12.7	5	2	28.3	22.2	27.3	27.09	21.6	29.4
				[0/90/0]s				
6.35	1	6	14.88	14.52	2.5	14.88	14.48	2.7
6.35	2	4	6.175	5.820	6.1	6.163	5.796	6.3
6.35	5	3	2.794	2.496	12.0	2.790	2.487	12.2
12.7	1	5	88.22	86.35	2.2	88.25	85.67	3.0
12.7	2	4	34.72	32.92	5.5	34.66	32.58	6.4
12.7	5	3	16.29	14.65	11.2	16.27	14.50	12.2

Fig. 6 Three dimensional mesh of cylindrical shell

According to Table 1, the calculated buckling loads for two states have been obtained which are in accordance with the results of Cagdas and Adali (2011). The minor differences of estimated buckling load under follower pressure between these studies are mainly due to different shell theories taken into account in the analyses. Gadgdas and Adali (2011) Extracted the relation for pressure stiffness according Koiter's (1967) assumption that is more useful for thin shell instability while in this study the assumptions used to derive the pressure stiffness, dose not restricted to thin or thick shells.

3.2 Comparison results

In this section, the accuracy of presented theory has been investigated. Hence, the results of this study have been compared with the results concluded by Asadi *et al*. (2012), Asadi and Qatu (2012) and Asadi and Qatu (2013) who used three dimensional elasticity and first order shear deformation shell theory by Qatu (FSDTQ) in order to execute static analysis of thick-deep laminated cylindrical shells. In this study, the mentioned element has been utilized to calculate the buckling pressure. In addition, the results were achieved for two-ply anti-symmetric [90/0] shells and by considering different thickness ratios (*a/h*) and depth ratios (*a/R*). Fig. 6 illustrates the mesh pattern of a typical cylindrical shell simulated by FEM which has used 3D elements.

It should be mentioned that in this example, the properties of material has been considered as follows:

$$E_{11}/E_{22} = 25 \quad G_{12}/E_{22} = 0.5 \quad G_{23}/E_{22} = 0.2 \quad G_{12} = G_{13} \quad \upsilon_{12} = 0.25$$

Table 2 represents dimensionless displacement, force and moment resultants at the center of shells, buckling pressure with different thickness ratios; moreover, *a/h*=10 and 20 describe moderately thick and thin shells, respectively. It also shows that results for three different depth ratios in which *a/R*=0.5, 1, and 2 representing shallow, deep, and very deep shells, respectively. Dimensionless transverse displacement, moment, force resultants and buckling pressure can be calculated by Eq. (28)

$$\begin{aligned} \bar{w} &= 10^3 E_{22} h^3 w / qa^4 \\ \bar{M} &= 10^3 M / qa^2 \\ \bar{N} &= 10^3 N / qa^3 \\ \bar{P} &= P R^3 / E_{22} h^3 \end{aligned} \tag{28}$$

Table 2 Comparison of dimensionless displacements, moments, force resultants and buckling pressure as in Eq. (28) of [0/90] cylindrical shells

a/h	*a/R*		$\bar{w}$	$\bar{M}$	$\bar{N}$	$\bar{P}$
10	0.5	FSDQT	11.636	52.822	1083.4	—
		3D	11.612	53.689	1084.7	0.3428
		Present study	11.852	55.291	1110.5	0.3482
	1	FSDQT	5.6735	31.043	1067	—
		3D	5.6746	31.638	1070.5	0.3165
		Present study	5.8434	32.386	1090.6	0.3229
	2	FSDQT	1.7089	12.899	658.02	—
		3D	1.7106	13.25	661.99	0.2865
		Present study	1.7501	13.484	670.39	0.2934
20	0.5	FSDQT	17.188	63.16	394.21	—
		3D	17.009	64.496	393.25	0.3621
		Present study	17.248	66.544	403.77	0.3699
	1	FSDQT	12.751	52.616	594.33	—
		3D	12.679	54.318	595.02	0.3309
		Present study	12.93	55.603	611.27	0.3378
	2	FSDQT	5.9488	30.132	568.08	—
		3D	5.9629	31.668	574.34	0.3110
		Present study	6.056	32.357	586.8	0.3168

According to Table 2, it can be concluded that the considered assumptions in this study are reasonable so that the maximum that have used three dimensional elements are estimated as: 2.975% for the displacement, 2.675% and 3.176% for force and moment, and 2.4% for buckling load relative differences of the current results and those of other researches of cylindrical shell under lateral pressure.

3.3 Buckling analysis of laminated cylindrical shell under follower pressure acting on neutral fiber and external fiber

In this section, the effect of follower forces is studied by considering the presence and absence of loading on neutral axis. Therefore, the buckling of cylindrical composite shells with simply supported ends under lateral pressure has been calculated. In addition, three different lengths to radius ratios which are 1, 2, 5 as well as different thicknesses being equal to 6.35, 12.7, 19.05, 25.4, 31.75, 38.1 mm have been considered. The maximum *L/h* utilized in the current analysis is 5. For larger ratios the suitable analysis can be a 3D analysis and using solid element or using HSDT shell theory for very deep shell such as the theory presented in Yaghoubshahi *et al*. (2011). Table 3 and Table 4 represent the results of analyses for lay-ups ($[90/90/90/]_s$, $[0/90/0]_s$). These tables give the calculated buckling pressure for the load is subjected to external fiber of the shell and the buckling pressure for the state when loading is subjected to neutral axial. The material in this example is Graphite/epoxy which its properties have been considered as follows:

$$E_{11} = 130 \text{ GPa} \quad E_{22} = 7 \text{ GPa} \quad G_{12} = G_{13} = 6 \text{ GPa}$$
$$G_{23} = 4.2 \text{ GPa} \quad \upsilon_{12} = \upsilon_{13} = 0.28 \quad \upsilon_{23} = 0.4$$

Table 3 Comparison of buckling pressure (MPa) of $[90]_6$ cylindrical shells for $z=0$ and $z=h/2$

h (mm)	L/R	Non-Follower ($z=0$)	Follower ($z=0$)	Follower ($z=h/2$)	n (circum. wave No.)
6.35	1	7.065	6.891	6.809	6
6.35	2	3.935	3.785	3.768	5
6.35	5	2.064	1.840	1.839	3
12.7	1	43.051	41.544	40.192	5
12.7	2	20.634	19.441	19.135	4
12.7	5	10.593	9.445	9.421	3
19.05	1	127.650	122.960	115.480	5
19.05	2	58.119	52.410	50.791	3
19.05	5	31.022	27.672	27.481	3
25.4	1	273.400	262.780	242.730	5
25.4	2	111.740	100.810	97.579	3
25.4	5	62.377	47.550	47.196	2
31.75	1	480.740	460.980	418.520	5
31.75	2	189.050	170.610	163.830	3
31.75	5	98.577	75.214	74.481	2
38.1	1	741.830	709.700	642.770	5
38.1	2	290.700	262.360	250.880	3
38.1	5	146.510	111.900	110.620	2

Table 4 Comparison of buckling pressure (MPa) of $[0/90/0/]_s$ cylindrical shells for $z=0$ and $z=h/2$

h (mm)	L/R	Non-Follower ($z=0$)	Follower ($z=0$)	Follower ($z=h/2$)	n (circum. wave No.)
6.35	1	11.716	11.530	11.476	6
6.35	2	5.451	5.252	5.243	5
6.35	5	2.216	1.981	1.978	3
12.7	1	65.270	64.026	63.359	5
12.7	2	31.323	29.711	29.586	4
12.7	5	12.059	10.761	10.743	3
19.05	1	170.830	167.140	164.040	5
19.05	2	81.583	77.342	76.968	3
19.05	5	35.331	31.511	31.427	3
25.4	1	324.580	317.200	311.040	5
25.4	2	160.110	151.750	150.860	3
25.4	5	75.706	66.230	65.902	2
31.75	1	521.120	508.650	498.150	5
31.75	2	264.120	250.310	247.400	3
31.75	5	128.710	101.990	101.310	2
38.1	1	748.680	731.590	715.240	5
38.1	2	388.610	368.270	363.420	3
38.1	5	186.450	147.620	146.350	2

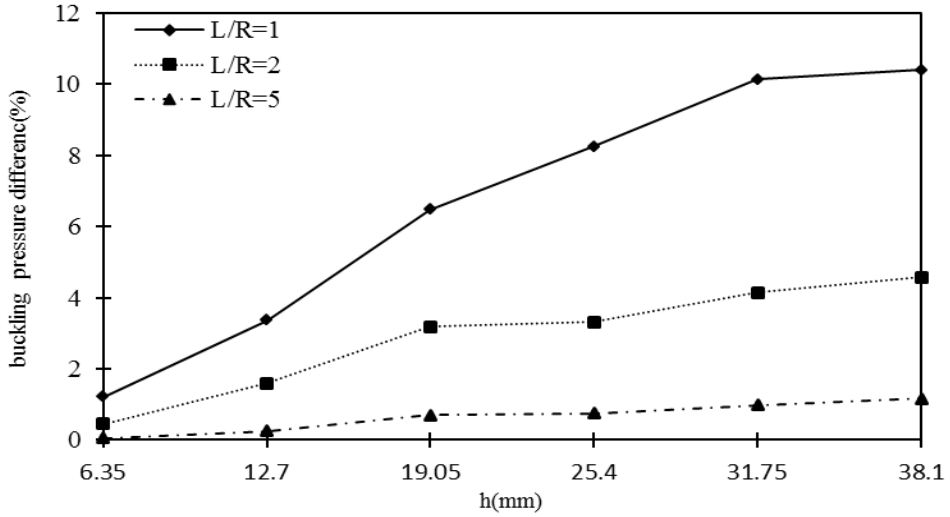

Fig. 7 difference of buckling pressure due to applying load on neutral axis and external fiber of $[90/90/90/]_s$ cylindrical shells

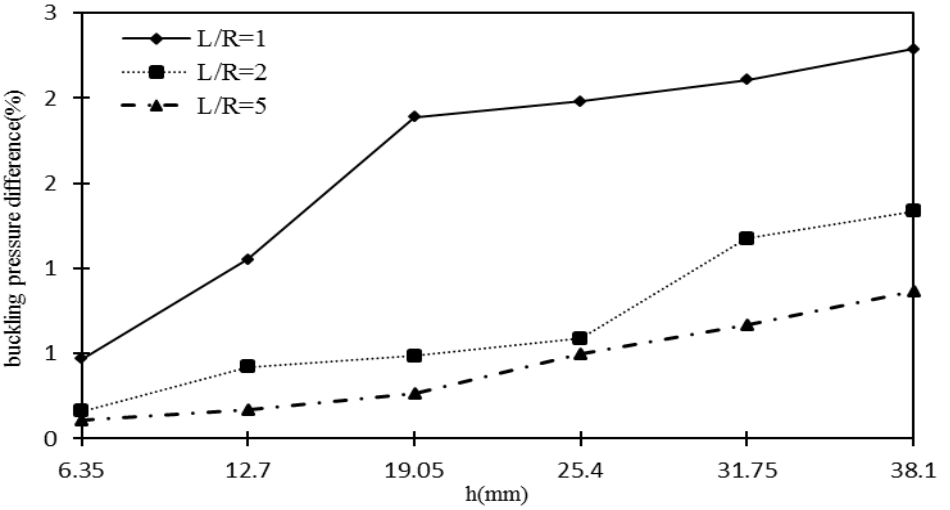

Fig. 8 difference of buckling pressure due to applying load on neutral axis and external fiber of $[0/90/0]_s$ cylindrical shells

By considering the presented results, since it has been assumed that the loading is non-follower forces in the thick cylindrical shells, the calculated buckling load increases rather than the state which the forces are dependent on deformation. Therefore, the comparison of the results reveals that for both follower and non-follower states, the difference between calculated buckling loads depends on different factors such as shell geometry so that if the thickness or length to radius ratio increases, the differences escalate. On the other hand, as it has been mentioned in this article, another assumption has been made in which the loads are subjected to neutral axis and external fiber of shell. Therefore, the results demonstrate that when a follower force is subjected to external

fiber, the buckling load decreases in comparison with the state that the load is subjected to neutral axis. As a result, the assumptions of non-follower pressure and loading on neutral fiber can lead to inaccurate results. Fig. 7 and Fig. 8 illustrate the relative differences of loading on neutral axis and external fiber for different thicknesses and layers.

Regarding the Figs. 7 and 8, the reader can conclude that when the shell thickness increases, the effect of loading on outer fiber is intensified and this outcome is true for thick shells. Consequently, the effect of loading on outer fiber decreases, if the length to radius ratio increases. This happens can be created by reducing displacements along the shells when the mentioned ratio increases.

In later problems (sections 3.4, 3.5 and 3.6), it is assumed that the loads which depend on deformation are subjected to outer shell fiber.

3.4 Buckling analysis of laminated cylindrical shell under hydrostatic follower pressure

In this case study, the effect of pressure stiffness (PS) on buckling load for composite cylindrical shells will be studied. Hence, a shell, with simply supported ends, is subjected to hydrostatic pressure. The radius of cylindrical shell equals to 100 millimeter (R=100 mm) and the studied thicknesses for two different states are 1.5 and 2 mm. It should be mentioned that the length to radius ratio has been considered 4 and 6. The regarded layers follow $[\theta/-\theta/\theta]_s$ rules in which $0\leq\theta\leq90$. To create hydrostatic pressure in this example, the axial and lateral loadings are subjected to the shell, simultaneously. Therefore, it is assumed that the shell is under the liquid by considering a deep depth. The lateral pressure is a ratio of axial pressure which can be calculated by using Eq. (29).

$$q = \frac{2}{R}P \tag{29}$$

The mechanical properties of material have been considered as follows:

$$E_{11} = 130\ \text{GPa} \quad E_{22} = 7\ \text{GPa} \quad G_{12} = G_{13} = 6\ \text{GPa}$$
$$G_{23} = 4.2\,\text{GPa} \quad \upsilon_{12} = \upsilon_{13} = 0.28 \quad \upsilon_{23} = 0.4$$

The results are presented in Tables 5(a)-(d).

Table 5(a) buckling pressure (MPa) of cylindrical under hydrostatic pressure for h=1.5 mm, L/R=4

Lay-up	Without (PS)	with (PS)	μ
$[0]_6$	28.842	26.323	9.57
[10/-10/10]s	34.765	31.741	9.53
[20/-20/20]s	50.27	45.634	10.16
[30/-30/30]s	71.369	64.125	11.30
[40/-40/40]s	98.939	88.665	11.59
[50/-50/50]s	133.75	111.16	20.32
[60/-60/60]s	138.07	108.81	26.89
[70/-70/70]s	139.06	110.45	25.90
[80/-80/80]s	140.36	111.55	25.83
[90/-90/90]s	140.42	111.31	26.15

Table 5(b) buckling pressure (MPa) of cylindrical under hydrostatic pressure for h=1.5 mm, L/R=6

Lay-up	Without (PS)	with (PS)	μ
$[0]_6$	21.516	19.589	9.84
[10/-10/10]s	24.575	22.351	9.95
[20/-20/20]s	33.904	30.688	10.48
[30/-30/30]s	51.371	46.108	11.41
[40/-40/40]s	68.291	52.594	29.85
[50/-50/50]s	79.709	61.861	28.85
[60/-60/60]s	95.578	74.767	27.83
[70/-70/70]s	110.98	87.299	27.13
[80/-80/80]s	121.98	96.196	26.80
[90/-90/90]s	126.02	99.413	26.76

Table 5(c) buckling pressure (MPa) of cylindrical under hydrostatic pressure for h=2 mm, L/R=4

Lay-up	Without (PS)	with (PS)	μ
$[0]_6$	60.510	55.591	8.85
[10/-10/10]s	71.345	65.580	8.79
[20/-20/20]s	101.070	92.384	9.40
[30/-30/30]s	144.460	130.630	10.59
[40/-40/40]s	201.680	181.690	11.00
[50/-50/50]s	259.310	217.530	19.21
[60/-60/60]s	264.210	208.550	26.69
[70/-70/70]s	273.290	219.090	24.74
[80/-80/80]s	279.340	224.870	24.22
[90/-90/90]s	280.960	223.610	25.65

Table 5(d) buckling pressure (MPa) of cylindrical under hydrostatic pressure for h=2 mm, L/R=6

Lay-up	Without (PS)	with (PS)	μ
$[0]_6$	47.216	43.184	9.34
[10/-10/10]s	53.341	48.927	9.02
[20/-20/20]s	72.917	66.544	9.58
[30/-30/30]s	110.240	99.134	11.20
[40/-40/40]s	132.950	103.390	28.59
[50/-50/50]s	163.220	127.710	27.81
[60/-60/60]s	198.890	156.600	27.01
[70/-70/70]s	230.970	182.620	26.48
[80/-80/80]s	252.920	200.380	26.22
[90/-90/90]s	260.900	206.780	26.17

According to Tables 5(a)-(d), it is clear that the maximum effect of follower force on the calculated buckling load for hydrostatic pressure is approximately 30% and this means that if the pressure stiffness matrix (deformation-dependent pressure effect) is neglected, the shell resistance

to buckling pressure could be overestimated up to thirty percent. It is also concluded that in the thick shells, the influence of pressure stiffness on buckling load increases when the length to radius ratio increases. On the other hand, this value decreases when the shell thickness increases. By considering the data, the μ=9.53% when h=1.5 mm, L/R=4 and θ=10 while for h= 2 mm, same L/R and θ=10, the value of μ decreases. In addition, another point is that the differences in calculated buckling loads caused by pressure stiffness effects are so that if the lay-up angle increases, then the μ increases as well.

3.5 Buckling analysis of laminated conical shell

In this example, the buckling load in truncated conical shells under the displacement-dependent hydrostatic pressure is investigated. Therefore, lay-ups $([60/-60/60]_s$, $[45/-45/45]_s)$ and Kevlar/ Epoxy material have been utilized. The conical shells have simply supported ends in the cone's end which is subjected to axial forces. The geometric properties of the shell have been illustrated in Fig 9. In addition, the mechanical properties of the material are considered as follows:

$$E_{11} = 80 \text{ GPa} \quad E_{22} = 6 \text{ GPa} \quad G_{12} = G_{13} = 2 \text{ GPa} \quad G_{23} = 1.5 \text{GPa} \quad \upsilon_{12} = \upsilon_{13} = 0.34 \quad \upsilon_{23} = 0.5$$
$$R_{Top} = 100 \text{mm}$$

The results are presented in Tables 6 and 7.

By considering the calculated results, for follower and non-follower forces, the calculated buckling load increases under hydrostatic pressure if the apex cone angle augments. Accordingly, in such case, the effect of pressure stiffness (μ) on buckling load increases for thick frustum shells if the apex cone angle or the thickness become larger. Whereas, for a constant apex cone angle and thickness, by increasing the length to radius ratio, the pressure stiffness decreases.

3.6 Buckling analysis of laminated shell of revolution

In this section, using the meridional equations, the buckling load is studied for rotating shells. These shells can be categorized into three different groups: firstly, the shells with positive Gaussian curvature in which two centers of curvature locate in one side such as Spherical, and

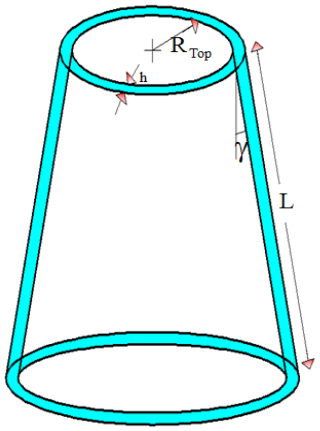

Fig. 9 geometry of conical shell

Table 6 buckling pressure of conical shell (MPa) of $[60/-60/60]_s$

h	*L/R*	Non-Follower	Follower	μ	Non-Follower	Follower	μ	Non-Follower	Follower	μ
	γ	30			45			60		
15	2	25.789	24.629	4.71	39.952	38.029	5.06	57.880	55.043	5.15
	5	3.835	3.724	2.99	7.528	7.262	3.65	13.429	12.677	5.93
	10	0.854	0.839	1.78	1.803	1.763	2.30	3.552	3.423	3.78
20	2	54.672	51.908	5.32	77.422	73.362	5.53	106.960	101.190	5.70
	5	7.760	7.490	3.61	14.924	14.191	5.17	26.169	24.620	6.29
	10	1.738	1.702	2.09	3.621	3.510	3.18	7.237	6.885	5.11
30	2	151.110	140.800	7.32	182.630	168.390	8.46	232.730	214.150	8.68
	5	20.369	19.318	5.44	38.305	36.093	6.13	65.277	61.115	6.81
	10	4.713	4.569	3.16	9.743	9.300	4.76	18.704	17.640	6.03

Table 7 buckling pressure of conical shell (MPa) of $[45/-45/45]_s$

h	L/R	Non-Follower	Follower	μ	Non-Follower	Follower	μ	Non-Follower	Follower	μ
	γ	30			45			60		
15	2	22.762	21.781	4.50	40.179	37.912	5.98	62.745	58.741	6.82
	5	4.310	4.187	2.92	8.994	8.622	4.32	16.454	15.558	5.76
	10	1.027	1.010	1.72	2.239	2.179	2.78	4.583	4.380	4.63
20	2	44.447	41.980	5.88	73.892	69.331	6.58	111.970	104.490	7.16
	5	8.429	8.149	3.45	17.177	16.353	5.04	31.641	29.811	6.14
	10	2.047	2.006	2.00	4.441	4.309	3.06	9.014	8.552	5.41
30	2	107.520	99.794	7.74	161.730	149.070	8.49	229.620	211.290	8.68
	5	21.709	20.597	5.40	42.175	39.822	5.91	75.804	70.201	7.98
	10	5.340	5.182	3.05	11.533	11.020	4.66	22.946	21.679	5.84

Parabolic shells. Secondly, negative Gaussian curvature shells which the both center of curvature are not located in the same side such as hyperbola shells. Finally, Zero Gaussian curvature shells which one of the curvature equals to zero such as cylindrical and conical shells. A catenary shell which its generator equation can be defined by Eq. (30) is illustrated in Fig. 10 (Tornabene 2011).

$$Z = d(\cosh(\frac{R_2 - R_b}{d}) - 1) \tag{30}$$

where *d* is the curvature radius in the apex of catenary curve. First and second curvature radii are also calculated by Eq. (31).

$$\begin{aligned} R_1 &= d\,\text{arcsin}\,h(\tan\varphi) + R_b \\ R_2 &= \frac{d}{\cos^2\varphi} \end{aligned} \tag{31}$$

Parametric meridional equation of cycloid curve is represented in Eq. (32). (Fig. 11)

$$\begin{aligned} Z &= r_c(1-\cos 2\varphi) \\ R &= r_c(2\varphi + \sin 2\varphi) + R_b \end{aligned} \tag{32}$$

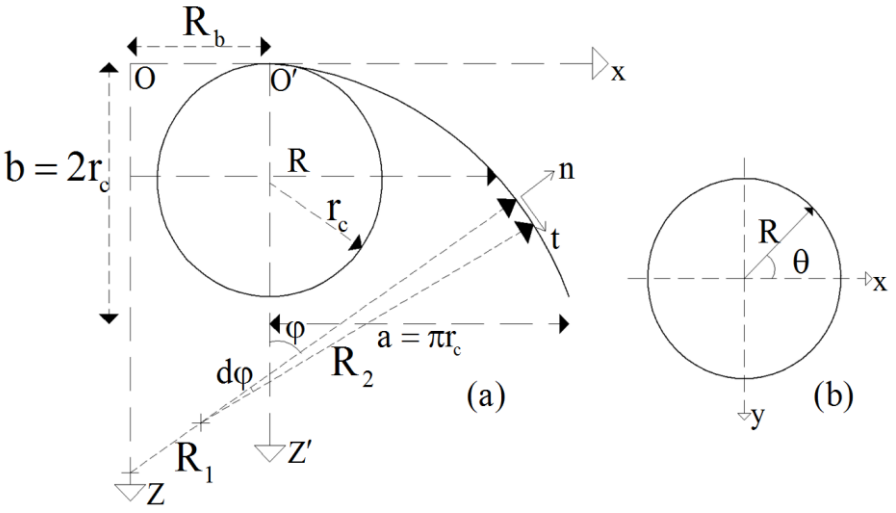

Fig. 11 cycloid shell geometry: (a) meridional section; (b) circumferential section

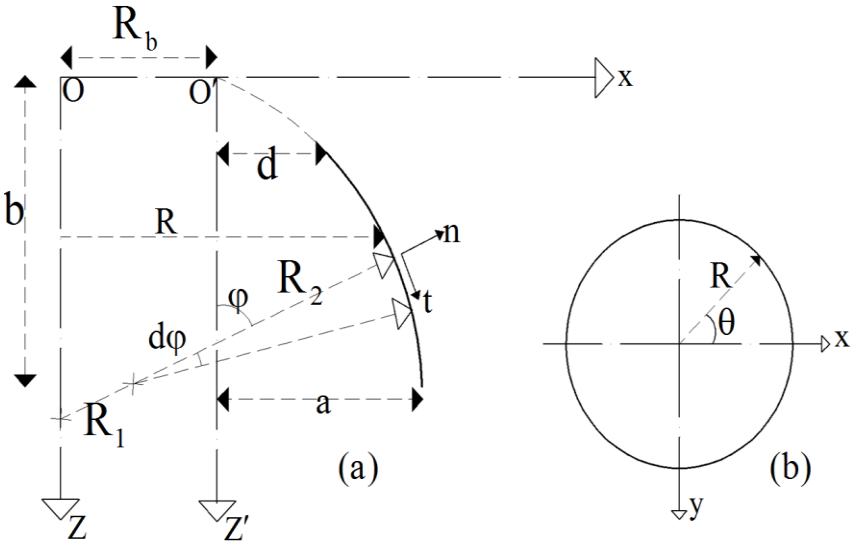

Fig. 12 parabolic shell geometry: (a) meridional section; (b) circumferential section

In this equation, r_c is the radius of the circle which have created cycloid curve. The radius of curvature in both circumferential and meridional directions is calculated by the Eq. (33).

$$R_1 = 4r_c \cos\varphi$$
$$R_2 = \frac{r_c(2\varphi + \sin 2\varphi) + R_b}{\sin\varphi} \tag{33}$$

The meridional equation of parabolic curve is presented in Eq. (34): (Fig. 12)

$$(R - R_b)^2 - kZ = 0 \tag{34}$$

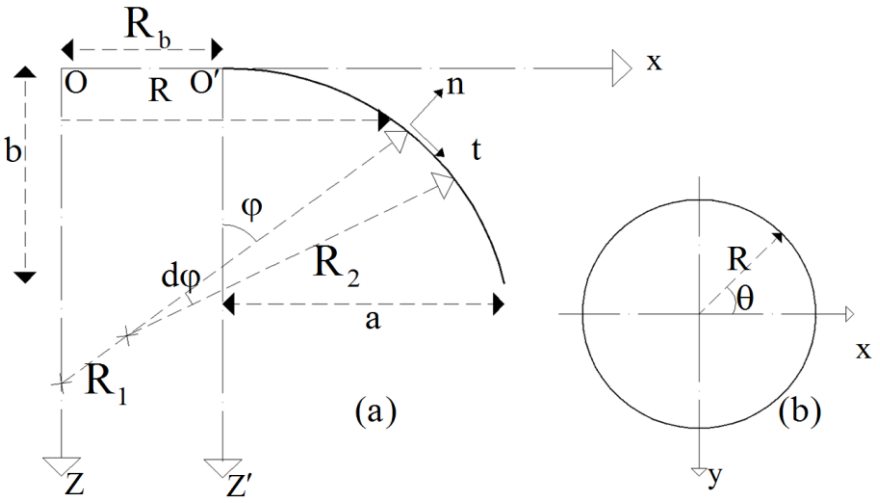

Fig. 13 elliptic shell geometry: (a) meridional section; (b) circumferential section

where in this equation, $k = \frac{a^2 - b^2}{b}$ represents the characteristic parameter of parabolic curve. The radii of curvature of parabolic shell are defined as

$$R_1 = \frac{k}{2\cos^2\varphi}$$
$$R_2 = \frac{k}{2\cos\varphi} + \frac{R_b}{\sin\varphi} \tag{35}$$

The meridional section of elliptical shell can be defined as below: (Fig. 13)

$$(R - R_b)^2 - k^2(b - Z)^2 = a^2 \tag{36}$$

where *a,b* and *k=a/b* are the semimajor and semiminor axes of the elliptic curve and their ratio, respectively. The first and second radii of curvature are calculated by utilizing the Eq. (37)

$$R_1 = \frac{ak}{\cos^2\varphi\sqrt{(1 + k^2\tan^2\varphi)^2}}$$
$$R_2 = \frac{ak}{\cos\varphi\sqrt{1 + k^2\tan^2\varphi}} + \frac{R_b}{\sin\varphi} \tag{37}$$

In this example, the geometric characteristics of shells are evaluated by considering an assumption that contends the lateral areas caused by different meridional curves are identical. In this problem, the lateral area and thickness are 60000 π mm^2 and 15 mm, respectively. Eq. (38) presents a formulation to calculate the lateral area

$$A = 2\pi\int_{\varphi_1}^{\varphi_2} R_1 R_2 \sin\varphi \, d\varphi \tag{38}$$

Table 8 Geometry of shell

Geometric properties	Geometry of shell
L=300 R=100	Cylindrical
R=173.205	Spherical
R_{bot}=200 R_{top}=0 L=300	Conical
a=190.5 b=139.35	Elliptic
a=225.892 d=100	Parabolic
z=300 d=134.868	Catenary
τ_c=64.40215	Cycloid

Table 9 buckling of shells of revolution (MPa)

Geometry	$[0/90/0]_s$			$[-45/45/-45]_s$			$[-45/45/-45]_2$		
	Non-Follower	follower	μ	Non-Follower	follower	μ	Non-Follower	follower	μ
Cylindrical	69.262	52.640	31.577	58.273	43.596	33.666	55.657	41.924	32.756
Spherical	278.050	234.120	18.764	221.63	186.1905	19.034	202.99	171.248	18.536
Conical	85.934	71.235	20.635	119.41	97.58749	22.362	113.42	93.194	21.703
Elliptic	153.060	131.209	16.654	120.42	102.5803	17.391	109.91	93.938	17.003
Parabolic	115.460	99.147	16.453	92.726	79.22523	17.041	85.108	72.953	16.662
Cycloid	144.460	126.981	13.765	113.96	98.90816	15.218	104.17	90.733	14.81
Catenary	72.952	63.616	14.675	82.006	70.52824	16.274	76.773	66.607	15.262

The Geometric properties of different shells with same volume are presented in Table 8.
The mechanical properties of the material are considered as below:

$$E_{11} = 149.66 \text{ GPa} \quad E_{22} = 9.93 \text{GPa} \quad G_{12} = G_{13} = G_{23} = 4.48162 \text{ GPa} \quad \upsilon_{12} = 0.28$$

Table 9 represents the calculated buckling loads for 7 different rotating shells and 2 symmetric lay-ups $[0/90/0]_s$, $[-45/45/-45]_s$ and a non-symmetric lay-up $[-45/45/-45]_2$. The boundary conditions of the shells are free supported in one end and fixed in another one. These shells are subjected to lateral uniform pressure.

By considering Table 9 it can be concluded that the procedure for the thick shells with positive and zero curvatures and identical lateral surfaces, the spherical and cylindrical shells have the most and the least buckling loads, respectively. Moreover, the pressure stiffness (μ) plays an important role in buckling load of shells. In the considered shells, the pressure stiffness leads to reduce the buckling pressure for cylindrical, conical, spherical, elliptical, catenary, and cycloid shell, respectively. To explain this phenomenon, it can be mentioned that the maximum displacement in circumferential direction occurs in cylindrical shells. In other words, when circumferential displacement increases, then normal angle of shell, before and after the deformation, augments. Consequently, owing to the same direction of pressure and normal vectors of shell, before and after deformation, the subjected pressure possess more effects on buckling load with respect to the case when the pressure is not dependent on deformations.

4. Conclusions

This work is devoted to the buckling behavior of laminated composite deep as well as thick shells of revolution under follower forces which remain normal to the shell. In order to obtain the results, the shell is divided into several closed strips being aligned with their nodal lines in the circumferential direction. The governing equations are derived based on first-order shear deformation theory which accounts for through thickness shear flexibility. Displacements and rotations in the shell middle surface are approximated by combining polynomial functions in the meridional direction and truncated Fourier series using appropriate number of harmonic terms in the circumferential direction. The load stiffness matrix is derived for each strip and assembled to form global load stiffness matrix of the shell, which may be un-symmetric. Upon forming linear elastic stiffness matrix also called constitutive stiffness matrix, geometric stiffness matrix, load stiffness matrix, the required elements for the second step analysis, which is an eigenvalue problem are provided. The numerical results support the following conclusions:

- All of the assumptions in this paper result in a reasonable accuracy for different shells, loading, materials in presence or absence of the pressure stiffness effect.
- The results for laminated shells of revolution show, when the pressure stiffness effect is included, this effect can result in reduction of the critical load as calculated without this effect. Therefore, it is considered that the assumption of loads which remain constant direction during deformations can lead to inaccurate results.
- Follower forces which are subjected to external fiber of thick shell can result in reduction in calculated buckling load. This effect can be intensified by increasing the thickness of the shell.
- If the thickness of thick shell increases, the effect of live pressure in calculated buckling load increases. In addition, the value increases with the length to radius ratio.
- The pressure stiffness effect which is related to the apex angle of conical shells under hydrostatic pressure is such that if the apex angle and thickness increases, pressure stiffness effect on buckling load augments as well.
- For the thick shells with positive and zero curvatures and identical lateral surfaces, the spherical and cylindrical shells have the most and the least buckling loads, respectively. In the considered loads, the pressure stiffness lead to reduce the buckling pressure for cylindrical, conical, spherical, elliptical, catenary, and cycloid shell, respectively.

References

ABAQUS/standard user's manual (1998), Vols. I-III, Version 5.8, Pawtucket, RI: Hibbitt, Karlsson & Sorensen, Inc.

Altman, W. and Oliveira, M.G.D. (1988), "Vibration and Stability cantilevered cylindrical shell panels under follower forces", *J. Sound Vib.*, **122**(2), 291-298.

Altman, W. and Oliveira, M.G.D. (1990), "Vibration and Stability shell panels with slight internal damping under follower forces", *J. Sound Vib.*, **136**(1), 45-50.

Argyris, J.H. and Symeonidis, S. (1981), "Nonlinear finite element analysis of elastic system under nonconservative loading - natural formulation, part 1, quasistatic problems", *Comput. Meth. Appl. Mech. Eng*., **26**, 75-123.

Asadi, E. and Qatu, M.S. (2012), "Static analysis of thick laminated shells with different boundary conditions using GDQ", *Thin Wall. Struct.*, **51**, 76-81.

Asadi, E. and Qatu, M.S. (2013), "Free vibration of thick laminated cylindrical shells with different

boundary conditions using general differential quadrature", *J. Vib. Control*, **19**(3), 356-366.
Asadi, E., Wang, W. and Qatu, M.S. (2012), "Static and vibration analyses of thick deep laminated cylindrical shells using 3D and various shear deformation theories", *Compos. Struct.*, **94**(2), 494-500.
Bolotin, V.V. (1963), *Nonconservative Problems Of The Theory Of Elastic Stability*, Pergamon Press, New York, NY, USA.
Cagdas, I.U. and Adali, S. (2011), "Buckling of cross-ply cylinders under hydrostatic pressure considering pressure stiffness", *Ocean Eng.*, **38**(4), 559-569.
Casimir, J.B., Nguyen, M.C. and Tawfiq, I. (2007), "Thick shells of revolution: Derivation of the dynamic stiffness matrix of continuous elements and application to a tested cylinder", *Comput. Struct.*, **85**(23-24), 1845-1857.
Chao, C.C., Tung, T.P. and Chern, Y.C. (1988), "Buckling of thick orthotropic spherical shells", *Compos. Struct.*, **9**(2)**,** 113-137.
Chen, J., Dawe, D.J. and Wang, S. (2000), "Nonlinear transient analysis of rectangular composite laminated plates", *Compos. Struct.*, **49**(2), 129-139.
Chen, W. and Zhang, W. (1993), "Buckling analysis of ring-stiffened cylindrical shells by compound strip method", *12th International Conference Computational Mechanics*, Stuttgart, Germany, August.
Cohen, G.A. (1966), "Conservative of a normal pressure field acting on a shell", *AIAA J.*, **4**(10).
Dooms, D., Degrande, G., De Roeck, G. and Reynders, E. (2004), "Wind induced vibration of thin-walled cylindrical structures", *International Conference on Noise and Vibration Engineering*, Leuven, Belgium, September.
Fukuchi, N. and Tanaka, T. (2006), "Non-periodic motions and fractals of a circular arch under follower forces with small disturbances", *Struct. Eng. Mech.*, **6**(2), 87-101.
Goyal, V.K. and Kapania, R.K. (2008), "Dynamic stability of laminated beams subjected to nonconservative loading", *Thin Wall. Struct.*, **46**(12), 1359- 1369.
Heppler, G.R. and Hansen, J.S. (1986), "A mindlin element for thick and deep shells", *Comput. Meth. Appl. Mech. Eng.*, **54**(1), 21-47.
Hibbitt, H.D. (1979), "Some follower forces and load stiffness", *Int. J. Numer. Meth. Eng.*, **14**(6), 207-23.
Iwata, K., Tsukimor, K. and Kubo, F. (1991), "A Symmetric Load-Stiffness Matrix for Buckling Analysis of Shell Structures under Pressure Loads", *Int. J. Press. Ves. Pip.*, **45**(1), 101-120.
Kang, J.H. (2012), "There-dimensional vibration analysis of joined thick conical-cylindrical shells of revolution with variable thickness", *J. Sound Vib.*, **331**(18)**,** 4187-4198.
Kang, J.H. (2015), "Vibrations of truncated shallow and deep conical shells with non-uniform thickness", *Struct. Eng. Mech.*, **55**(1), 29-46.
Kang, J.H. and Leissa, A.W. (2005), "Three-dimensional vibration analysis of thick hyperboloidal shells of revolution", *J. Sound Vib.*, **282**(1-2), 277-296.
Kasagi, A. and Sridharan, S. (1993), "Buckling and postbuckling analysis of thick composite cylindrical shells under hydrostatic pressure", *Compos. Eng.*, **3**(5), 467-481.
Koiter, W.T. (1967), *General Equations Of Elastic Stability For Thin Shells*, Theory of Thin Shells, Univ. of Houston Press, USA.
Lazzari, M., Vitaliani, R.V., Majowiecki, M. and Saett, A.V. (2003), "Dynamic behavior of a tensegrity system subjected to follower wind loading", *Comput. Struct.*, **81**(22-23), 2199-2217.
Lu, G. and Mao, R. (2001), "A study of the plastic buckling of axially compressed cylindrical shells with a thick-shell theory", *Int. J. Mech. Sci.*, **43**(10), 2319-2330.
Nali, P., Carrera, E. and Lecca, S. (2011), "Assessments of refined theories for buckling analysis of laminated plates", *Compos. Struct.*, **93**(2), 456-464.
Ovesy, H.R. and Fazilati, J. (2009), "Stability analysis of composite laminated plate and cylindrical shell structures using semi-analytical finite strip method", *Compos. Struct.*, **89**(3), 467-474.
Park, S.H. and Kim, J.H. (2002), "Dynamic stability of a stiff-edged cylindrical shell subjected to a follower force", *Comput. Struct.*, **80**(3-4), 227-233.
Poorveis, D. and Kabir, M.Z. (2006), "Buckling of discretely stringer-stiffened composite cylindrical shells under combined axial compression and external pressure", *Scientia Iranica*, **13**(2), 113-123.

Qatu, M.S. (1999), "Accurate equations for laminated composite deep thick shells", *Int. J. Solid. Struct.*, **36**(19), 2917-2941.
Romano, G. (1971), "Potential operators and conservative systems", *Proceedings of the 14th Polish Solid Mechanics Conference,* Kroscjenko, Poland, September.
Ross, C.T.F. and Little, A.P.F. (2007), "Design charts for the general instability of ring-stiffened conical shells under external hydrostatic pressure", *Thin Wall. Struct.*, **45**(2), 199-208.
Ross, C.T.F., Sawkins, D. and Johns, T. (1999), "A Inelastic buckling of thick-walled circular conical shells under external hydrostatic pressure", *Ocean Eng.*, **26**(12), 1297-1310.
Sanders, J. and Lyell, J. (1959), "An improved first-approximation theory for thin shells", NASA Technical Report, NASA-TR-R24.
Schweizerhof, K. and Ramm, E. (1984), "Displacement dependent pressure loads in nonlinear finite element analysis", *Comput. Struct.*, **18**(6), 1099-1114.
Sheinman, I. and Tene, Y. (1974), "Potential energy of a normal pressure field acting on an arbitrary shell", *AIAA J.*, **11**(8), 1216-1216.
Spagnoli, A. (2001), "Different buckling modes in axially stiffened conical shells", *Eng. Struct.*, **23**(8), 957-965.
Teng, J.G. and Hong, T. (1998), "Nonlinear thin shell theories for numerical buckling predictions", *Thin Wall. Struct.*, **31**(1-3), 89-115.
Thangam Babu, P.V. and Reddy, D.V. (1973), "Frequency analysis of orthotropic circular cylindrical panels by the finite strip method", *Build. Sci.*, **8**(3), 229-241.
Tornabene, F. (2011), "2-D GDQ solution for free vibrations of anisotropic doubly-curved shells and panels of revolution", *Compos. Sstruct.*, **93**(7), 1854-1876.
Tornabene, F. and Viola, E. (2008), "2-D solution for free vibrations of parabolic shells using generalized differential quadrature method", *Eur. J. Mech. A/Solid.*, **27**(6), 1001-1025.
Tornabene, F., Brischetto, S., Fantuzzi, N. and Viola, E. (2015), "Numerical and exact models for free vibration analysis of cylindrical and spherical shell panels", *Compos. Part B: Eng.*, **81**, 231-250.
Tornabene, F., Fantuzzi, N. and Bacciocchi, M. (2014), "Free vibrations of free-form doubly-curved shells made of functionally graded materials using higher-order equivalent single layer theories", *Compos. Part B: Eng.*, **67**, 490-509.
Tornabene, F., Fantuzzi, N. and Bacciocchi, M. (2014), "The local GDQ method applied to general higher-order theories of doubly-curved laminated composite shells and panels: The free vibration analysis", *Compos. Struct.*, **116**, 637-660.
Tornabene, F., Fantuzzi, N., Bacciocchi, M. and Dimitri, R. (2015), "Free vibrations of composite oval and elliptic cylinders by the generalized differential quadrature method", *Thin Wall. Struct.*, **97**, 114-129.
Tornabene, F., Fantuzzi, N., Bacciocchi, M. and Dimitri, R. (2015), "Dynamic analysis of thick and thin elliptic shell structures made of laminated composite materials", *Compos. Struct.*, **133**, 278-299.
Tornabene, F., Fantuzzi, N., Bacciocchi, M. and Viola, E. (2015), "Higher-order theories for the free vibrations of doubly-curved laminated panels with curvilinear reinforcing fibers by means of a local version of the GDQ method", *Compos. Part B: Eng.*, **81**, 196-230.
Tornabene, F., Fantuzzi, N., Bacciocchi, M. and Viola, E. (2015), "A new approach for treating concentrated loads in doubly-curved composite deep shells with variable radii of curvature", *Compos. Struct.*, **131**, 433-452.
Wang, J. and Schweizerhof, K. (1996), "Study on free vibration of moderately thick orthotropic laminated shallow shells by boundary domain elements", *Appl. Math. Model.*, **20**(8)**,** 579-584.
Wang, Q. (2003), "On complex flutter and buckling analysis of a beam structure subjected to static follower force", *Struct. Eng. Mech.*, **16**(5), 533-556.
Wang, S. Dawe, D.J. (1999), "Buckling of composite shell structures using the spline finite strip method", *Compos. Part B*, **30**(4), 351-364.
Wang, X.H. and Redekop, D. (2011), "Free vibration analysis of moderately-thick and thick toroidal shells", *Struct. Eng. Mech.*, **39**(4), 449-463.
Yaghoubshahi, M., Asadi, E. and Fariborz, S.J. (2011), "A higher- order shell model applied to shell with

mixed boundary condations", *Proceeding of The Institution of Mechanical Engineering, Part C*., **224.**
Zhong, W.X. and Cheung, Y.K. (1998), "The precise finite strip method", *Compos. Struct.***,** **69**(6), 773-783.

CC

Appendix A

As stated in the paper context, the elemental area of the shell deformed surface (dS^*) multiplied by the normal vector ($\vec{n}^*$) can be defined by the following vector product

$$dS^*\vec{n}^* = \frac{\partial \vec{R}^*}{\partial \theta} d\theta \times \frac{\partial \vec{R}^*}{\partial s} ds \tag{A1}$$

The expansion of Eq. (A1) can be defined by the following determinant

$$dS^*\vec{n}^* = \begin{vmatrix} \vec{i} & \vec{j} & \vec{k} \\ \left(\begin{array}{l} \frac{\partial u}{\partial s}\cos\theta\cos\varphi \\ -u\cos\theta\sin\varphi R_1^{-1} \\ +\frac{\partial w}{\partial s}\cos\theta\sin\varphi \\ +w\cos\theta\cos\varphi R_1^{-1} \\ -\frac{\partial v}{\partial s}\sin\theta+\frac{\partial R}{\partial s}\cos\theta \\ -z\frac{\partial \beta_s}{\partial s}\cos\varphi\cos\theta \\ +z\beta_s R_1^{-1}\sin\varphi\cos\theta \\ +z\frac{\partial \beta_\theta}{\partial \varphi}\sin\theta \end{array}\right) & \left(\begin{array}{l} \frac{\partial u}{\partial s}\cos\varphi\sin\theta \\ -u\sin\varphi\sin\theta * R_1^{-1} \\ +\frac{\partial w}{\partial s}\sin\varphi\sin\theta \\ +w\cos\varphi\sin\theta R_1^{-1} \\ +\frac{\partial v}{\partial s}\cos\theta+\frac{\partial R}{\partial s}\sin\theta \\ -z\frac{\partial \beta_s}{\partial s}\cos\varphi\sin\theta \\ +z\beta_s R_1^{-1}\sin\varphi\sin\theta \\ -z\frac{\partial \beta_\theta}{\partial s}\cos\theta \end{array}\right) & \left(\begin{array}{l} \frac{\partial u}{\partial s}\sin\varphi \\ +u\cos\varphi R_1^{-1} \\ -\frac{\partial w}{\partial s}\cos\varphi \\ +w\sin\varphi R_1^{-1} \\ +\frac{\partial Z}{\partial s}-z\frac{\partial \beta_s}{\partial s}\sin\varphi \\ -z\beta_s\cos\varphi R_1^{-1} \end{array}\right) \\ \left(\begin{array}{l} -R\sin\theta+\frac{\partial u}{\partial \theta}\cos\theta\cos\varphi \\ -u\cos\varphi\sin\theta \\ +\frac{\partial w}{\partial \theta}\sin\varphi\cos\theta \\ -w\sin\varphi\sin\theta \\ -\frac{\partial v}{\partial \theta}\sin\theta-v\cos\theta \\ -z\frac{\partial \beta_s}{\partial \theta}\cos\varphi\cos\theta \\ +z\beta_s\cos\varphi\sin\theta \\ +z\frac{\partial \beta_\theta}{\partial \theta}\sin\theta \\ +z\beta_\theta\cos\theta \end{array}\right) & \left(\begin{array}{l} R\cos\theta \\ +\frac{\partial u}{\partial \theta}\cos\varphi\sin\theta \\ +u\cos\varphi\cos\theta \\ +\frac{\partial w}{\partial \theta}\sin\varphi\sin\theta \\ -v\sin\theta \\ +w\sin\varphi\cos\theta \\ +\frac{\partial v}{\partial \theta}\cos\theta \\ -z\frac{\partial \beta_s}{\partial \theta}\cos\varphi\sin\theta \\ -z\beta_s\cos\varphi\cos\theta \\ -z\frac{\partial \beta_\theta}{\partial \theta}\cos\theta \\ +z\beta_\theta\sin\theta \end{array}\right) & \left(\begin{array}{l} \frac{\partial u}{\partial \theta}\sin\varphi \\ -\frac{\partial w}{\partial \theta}\cos\varphi \\ -z\frac{\partial \beta_s}{\partial \theta}\sin\varphi \end{array}\right) \end{vmatrix} dsd\theta$$

Appendix B

The expanded forms of F_u, F_v, F_w, $F_{\beta s}$ and $F_{\beta\theta}$ defined in the Eq. (22) are as follows

$$
\begin{aligned}
F_U = & -\frac{u^2\cos\varphi}{R_1} + v\frac{\partial v}{\partial s}\sin\varphi + R\frac{\partial w}{\partial s} - \frac{\partial v}{\partial s}\frac{\partial w}{\partial \theta} + \frac{\partial v}{\partial \theta}\frac{\partial w}{\partial s} + z\frac{\partial \beta_\theta}{\partial s}\frac{\partial w}{\partial \theta} \\
& -z\frac{\partial \beta_\theta}{\partial \theta}\frac{\partial w^1}{\partial s} - \frac{uR}{R_1} - (u\frac{\partial v}{\partial \theta})/R_1 + u\frac{\partial w}{\partial s}\cos\varphi + w\frac{\partial w}{\partial s}\sin\varphi \\
& -\beta_\theta z\frac{\partial v}{\partial s}\sin\varphi - zv\frac{\partial \beta_\theta}{\partial s}\sin\varphi + \beta_\theta z^2\frac{\partial \beta_\theta}{\partial s}\sin\varphi - \frac{uw\sin\varphi}{R_1} + \frac{\beta_s zR}{R_1} \\
& +(\beta_s z\frac{\partial v}{\partial \theta})/R_1 + (uz\frac{\partial \beta_\theta}{\partial \theta})/R_1 - \beta_s z\frac{\partial w}{\partial s}\cos\varphi \\
& -\frac{\beta_s^2 z^2\cos\varphi}{R_1} + \frac{2\beta_s uz\cos\varphi}{R_1} + \frac{\beta_s wz\sin\varphi}{R_1} - (\beta_s z^2\frac{\partial \beta_\theta}{\partial \theta})/R_1
\end{aligned}
$$

$$
\begin{aligned}
F_V = & -v\sin\varphi + v\frac{\partial w}{\partial s}\cos\varphi + \frac{\partial w}{\partial \theta} - v\frac{\partial u}{\partial s}\sin\varphi + \frac{\partial u}{\partial s}\frac{\partial w}{\partial \theta} - \frac{\partial u}{\partial \theta}\frac{\partial w}{\partial s} + \beta_\theta z\sin\varphi \\
& +u\frac{\partial u}{\partial \theta}/R_1 + w\frac{\partial w}{\partial \theta}/R_1 - \beta_\theta z\frac{\partial w}{\partial s}\cos\varphi + \beta_\theta z\frac{\partial u}{\partial s}\sin\varphi + vz\frac{\partial \beta_s}{\partial s}\sin\varphi \\
& -(uv\cos\varphi)/R_1 - (vw\sin\varphi)/R_1 - \beta_\theta z^2\frac{\partial \beta_s}{\partial s}\sin\varphi \\
& +(\beta_\theta uz\cos\varphi)/R_1 + (\beta_s vz\cos\varphi)/R_1 + (\beta_\theta wz\sin\varphi)/R_1 - (\beta_s\beta_\theta z^2\cos\varphi)/R_1 \\
& +(\beta_s z^2\frac{\partial \beta_s}{\partial \theta})/R_1 - (uz\frac{\partial \beta_s}{\partial \theta})/R_1 - (\beta_s z\frac{\partial u}{\partial \theta})/R_1 - (z\frac{\partial \beta_s}{\partial s}\frac{\partial w}{\partial \theta}) + z\frac{\partial \beta_s}{\partial \theta}\frac{\partial w}{\partial s}
\end{aligned}
$$

$$
\begin{aligned}
F_W = & -R - v\frac{\partial v}{\partial s}\cos\varphi - \frac{\partial v}{\partial \theta} - R\frac{\partial u}{\partial s} + \beta_\theta z\frac{\partial v}{\partial s}\cos\varphi + vz\frac{\partial \beta_\theta}{\partial s}\cos\varphi \\
& -u\cos\varphi + (\frac{\partial u}{\partial \theta}\frac{\partial v}{\partial s}) - (\frac{\partial u}{\partial s}\frac{\partial v}{\partial \theta}) - (\beta_\theta z^2\frac{\partial \beta_\theta}{\partial s}\cos\varphi)/R_1 - w\sin\varphi \\
& -(w^2\sin\varphi)/R_1 - Rw/R_1 - z^2\frac{\partial \beta_s}{\partial s}\frac{\partial \beta_\theta}{\partial \theta} + z^2\frac{\partial \beta_s}{\partial \theta}\frac{\partial \beta_\theta}{\partial s} - (u\frac{\partial u}{\partial s}\cos\varphi) \\
& -(w\frac{\partial u}{\partial s}\sin\varphi) + z\frac{\partial \beta_\theta}{\partial s} - z\frac{\partial \beta_\theta}{\partial s}\frac{\partial u}{\partial \theta} + z\frac{\partial \beta_\theta}{\partial \theta}\frac{\partial u}{\partial s} + z\frac{\partial \beta_s}{\partial \theta}\frac{\partial v}{\partial \theta} \\
& -z\frac{\partial \beta_s}{\partial \theta}\frac{\partial v}{\partial s} - (uw\cos\varphi)/R_1 - \beta_s z^2\frac{\partial \beta_s}{\partial s}\cos\varphi - (w\frac{\partial v}{\partial \theta})/R_1 - \beta_s z^2\frac{\partial \beta_s}{\partial s}\cos\varphi \\
& +\beta_s z\cos\varphi + (wz\frac{\partial \beta_\theta}{\partial \theta})/R_1 + Rz\frac{\partial \beta_s}{\partial s}/R_1 + (\beta_s wz\cos\varphi)/R_1 \\
& +wz\frac{\partial \beta_s}{\partial s}\sin\varphi + uz\frac{\partial \beta_s}{\partial s}\cos\varphi + \beta_s z\frac{\partial u}{\partial s}\cos\varphi
\end{aligned}
$$

$$
\begin{aligned}
F_{\beta_s} = & -z\frac{\partial v}{\partial \theta}\frac{\partial w}{\partial s} + z\frac{\partial v}{\partial s}\frac{\partial w}{\partial \theta} + \beta_s z^2\frac{\partial w}{\partial s}\cos\varphi - z^2\frac{\partial \beta_\theta}{\partial s}\frac{\partial w}{\partial \theta} \\
& +z^2\frac{\partial \beta_\theta}{\partial \theta}\frac{\partial w}{\partial s} + (u^2 z\cos\varphi)/R_1 - (vz\frac{\partial v}{\partial s}\sin\varphi)/R + (\beta_s^2 z^3\cos\varphi)/R_1 \\
& -Rz\frac{\partial w}{\partial s} - \beta_\theta z^3\frac{\partial \beta_\theta}{\partial s}\sin\varphi + \beta_\theta z^2\frac{\partial v}{\partial s}\sin\varphi - uz\frac{\partial w}{\partial s}\cos\varphi - wz\frac{\partial w}{\partial s}\sin\varphi \\
& +vz^2\frac{\partial \beta_\theta}{\partial s}\sin\varphi) - (uz^2\frac{\partial \beta_\theta}{\partial \theta})/R_1 + (Ruz)/R_1 + (uz\frac{\partial v}{\partial \theta})/R_1 + (uwz\sin\varphi)/R_1 \\
& -\beta_s Rz^2/R_1 - (2\beta_s uz^2\cos\varphi)/R_1 + (\beta_s z^3\frac{\partial \beta_\theta}{\partial \theta})/R_1 - (\beta_s z^2\frac{\partial v}{\partial \theta})/R_1 - (\beta_s wz^2\sin\varphi)/R_1
\end{aligned}
$$

$$
\begin{aligned}
F_{\beta_\theta} &= -\beta_\theta z^2 \sin\varphi - vz\sin\varphi - z\frac{\partial u}{\partial s}\frac{\partial w}{\partial \theta} + z\frac{\partial u}{\partial \theta}\frac{\partial w}{\partial s} + z^2\frac{\partial \beta_s}{\partial s}\frac{\partial w}{\partial \theta} - z^2\frac{\partial \beta_s}{\partial \theta}\frac{\partial w}{\partial s} \\
&-vz\frac{\partial w}{\partial s}\cos\varphi - z\frac{\partial w}{\partial \theta} + vz\frac{\partial u}{\partial s}\sin\varphi - (uz\frac{\partial u}{\partial \theta})/R_1 + (w\frac{\partial w}{\partial \theta}z)/R_1 \\
&-(\beta_s z^3\frac{\partial \beta_s}{\partial \theta})/R_1 + (\beta_s z^2\frac{\partial u}{\partial \theta})/R_1 + (uz^2\frac{\partial \beta_s}{\partial \theta})/R_1 + \beta_\theta z^2\frac{\partial w}{\partial s}\cos\varphi \\
&+\beta_\theta\frac{\partial \beta_s}{\partial s}z^3\sin\varphi - \beta_\theta z^2\frac{\partial u}{\partial s}\sin\varphi - vz^2\frac{\partial \beta_s}{\partial s}\sin\varphi + (uvz\cos\varphi)/R_1 \\
&+(vwz\sin\varphi)/R_1 + (\beta_\theta\beta_s z^3\cos\varphi)/R_1 - (\beta_\theta uz^2\cos\varphi)/R_1 - (\beta_s vz^2\cos\varphi)/R_1 \\
&-(\beta_\theta wz^2\sin\varphi)/R_1
\end{aligned}
$$